Multi-level optimisation of composite structures through a global-local modelling approach based on high-order theories

Marco Montemurro [a,*], Giacinto Alberto Fiordilino [a,b], Erasmo Carrera [b]

[a] *Arts et Métiers Institute of Technology, Université de Bordeaux, CNRS, INRA, Bordeaux INP, HESAM Université, I2M UMR 5295, F-33405 Talence, France*
[b] *MUL2 group, DIMEAS, Politecnico di Torino, Torino, Italy*

ABSTRACT

This paper presents an original multi-level optimisation method for the design of composite structures integrating a global–local approach based on higher-order theories to assess the responses of the structure at each scale. The method offers a good balance between accuracy and computational costs. Unlike multi-level strategies available in the literature, in the proposed approach there is a strong interaction between the steps of the optimisation process. The proposed method is articulated in two nested optimisation loops (outer and inner). The outer loop focuses on the macroscopic scale where the polar formalism is used to describe the laminate behaviour. The resolution of the outer loop is performed through a special metaheuristic algorithm. However, since requirements on local structural responses are evaluated on the most critical region of the structure (modelled through a higher-order theory) at the ply-level, for each solution of the outer loop, a nested genetic optimisation (inner loop) is performed to find the stack matching the values of the geometric variables and of the polar parameters corresponding to the current solution of the outer loop. During the inner loop, the optimised stacking sequences are searched in the domain of general quasi-trivial solutions, without introducing simplifying hypotheses.

The new methodology is applied to the least-weight design of a simplified wing-box structure by considering requirements of both mechanical nature (first buckling load, first-ply failure, and delamination) and technological nature (blending between adjacent laminates).

1. Introduction

Fibre-reinforced composite materials are widely used in different industrial fields thanks to their outstanding performances, e.g., high stiffness-to-weight and strength-to-weight ratios, which lead to a substantial weight saving when compared to metallic alloys. Moreover, nowadays, new classes of composite structures, like variable-stiffness composite structures [1–5] or multi-material structures [6,7], can be designed (through alternative approaches) and fabricated thanks to modern additive manufacturing processes for composite materials.

Nevertheless, the design of composite structures requires the formulation of a complex multi-scale problem involving a huge amount of design variables and a variety of phenomena intervening at different scales [8]. In the case of multilayer plates (which represent the main focus of this paper) the problem scales are, at least, three: (1) the microscopic scale (that of the constitutive phases), (2) the mesoscopic scale (that of the constitutive lamina) and (3) the macroscopic scale (that of the laminate).

Furthermore, the designer has to deal with design variables of different nature depending on the considered scale. At the microscopic scale, for instance, the design variable set includes the material properties of constitutive phases (fibres, matrix, additives, etc.), their volume fraction and the spatial distribution of each phase, i.e., the topology of the representative volume element. At the mesoscopic scale, the design variables are the material properties, the thickness and the orientation angle of the single lamina. At the macroscopic scale, the composite is often modelled as an equivalent homogeneous anisotropic medium whose mechanical behaviour is described in terms of a set of constitutive matrices, which depend on the choice of the kinematic model. For instance, in the framework of the classic laminate theory, two mathematical representations of the anisotropy of multilayer structures at the macroscopic scale can be found in the literature. The first one makes use of the well-known lamination parameters (LPs) coupled with the parameters of Tsai and Pagano, see [9–11]. These parameters unquestionably provide a compact representation of the stiffness tensors of the laminate, although they are not all tensor

* Corresponding author.
  E-mail addresses: marco.montemurro@ensam.eu, marco.montemurro@u-bordeaux.fr (M. Montemurro).

invariants [11]. The second one is represented by the polar formalism introduced by Verchery [12], and generalised to the case of higher-order equivalent single layer theories by Montemurro [13–15]. Thanks to the polar formalism it is possible to represent any plane tensor by means of tensor invariants, referred to as polar parameters (PPs), which are directly related to the symmetries of the tensor.

Nevertheless, regardless of the formalism adopted to represent the laminate anisotropy at the macroscopic scale, the design variables involved at different scales are related, and the relationship among the problem scales is not bijective [9]. Moreover, depending on the problem at hand, the design requirements are often defined at different scales, and the coupling among scales, which can be weak or strong, depends on the problem formulation too, thus, further complicating the design of composite structures [16]. The development of a suitable design strategy taking into account the above aspects is of paramount importance, although this task is anything but trivial.

Many researchers have faced the challenge of developing suitable strategies and algorithms for the design of composite structures and the research is still ongoing. Specifically, the formulation of the problem for searching the optimal stacking sequences can also be decisive. The literature survey done by Ghiasi et al. [8] exhaustively summarises the possible optimisation strategies (and the related problem formulation) by dividing them into two categories: single-level optimisation strategies (also refereed to as "direct approach") and multi-level optimisation strategies.

When adopting the first approach, the design problem is formulated by directly employing the number, thickness and orientation of plies as design variables. This approach allows for an easy implementation of many constraints and requirements. Nevertheless, it presents some shortcomings. Firstly, the optimisation problem formulated in the space of the plies orientations is highly non-convex and prone to converge towards local minima. This is due to the trigonometric functions involved in the definition of the stiffness matrices of the laminate. Secondly, to reduce the complexity of the solution search process, engineers systematically make use of simplifying hypotheses and design guidelines to find feasible solutions. In the literature, the most frequently used assumptions are about the nature of the stacking sequence [17,18]. Researchers usually make use of symmetric (a sufficient condition to ensure membrane/bending uncoupling) balanced (a sufficient condition to ensure a membrane orthotropic behaviour) stacks whose orientation angles take values in the following "canonical set": $0°, \pm45°, 90°$. Together with the above simplifying hypotheses a set of design rules [17,18] is often introduced when searching for an optimum stack: percentage rule, contiguity rule, disorientation rule, grouping rule, etc. These rules represent a sort of best practice

in designing conventional stacks, which are the result of the experience collected in the last 50 years in the aerospace sector. Although such rules allow simplifying the design problem of a composite structure, their systematic use has an important consequence: the extent of the design space is extremely shrunk and the number of potential optimal solutions is, thus, decreased. Finally, the number of design variables is not generally known a priori when optimising for lightness. Moreover, it is dramatically size-dependent, which makes the approach not suitable for the design of large structures [19,20]. The interested reader can find more details on the direct approach in [8].

To alleviate the drawbacks of the direct approach, in the multi-level optimisation strategies the design problem is split into two linked sub-problems, each one focusing on a different scale. The first-level problem (FLP) deals with the macroscopic scale and each laminate composing the structure is modelled as an equivalent homogeneous anisotropic medium. The design problem is solved by optimising the geometric variables of the structure and the parameters describing the macroscopic behaviour of the laminate, i.e., either the LPs or the PPs depending on the formalism adopted to represent the laminate anisotropy at this scale. Of course, all the requirements involved into the design problem should be taken into account at this level via a suitable formulation of equivalent constraints in the LPs space or in the PPs one (this task is anything but trivial). The second-level problem (SLP) focuses on the laminate mesoscopic scale and the goal is to recover at least one stacking sequence matching the optimised mechanical properties resulting from the FLP. The design variables of the SLP are the plies orientation angles (and sometimes their thickness).

The vast majority of the studies dealing with multi-level optimisation strategies makes use of the representation of anisotropy based on LPs. Diaconu et al. [21], provided the inequalities defining the laminate feasibility domain in the LPs space. Many research studies [17,18,22–30] took inspiration from this work and justify the use of the multi-level optimisation approach on the basis of the (presumed) convexity of the feasibility domain in the LPs space. Nevertheless, as recently rigorously proven by Picchi Scardaoni and Montemurro [31], the laminate feasibility domain in the LPs space (but also in the PPs space) is not convex for laminates with identical plies (i.e., plies made of the same material and thickness), thus, this argument cannot be used to justify the use of the multi-level optimisation approach. Among the works mentioned above, the one by Bramsiepe et al. [29] presented a multi-level optimisation approach based on LPs for the least-weight design problem of a lifting system structure made of symmetric laminates by considering design requirements on blending, buckling and failure constraints. The reader is addressed to the review article [32] to find further interesting works on multi-level optimisation strategies using LPs.

The multi-level optimisation approach based on the polar formalism is often referred to as multi-scale two-level optimisation strategy (MS2LOS). It has been originally introduced in [33,34] and has been later generalised, expanded and used in several works, like [35–42]. The MS2LOS based on the polar formalism is characterised by some interesting features (corresponding to just as many advantages): a general problem formulation (for both FLP and SLP), the absence of simplifying hypotheses on the nature of the stacking sequences, and the use of PPs to optimise locally the elastic symmetries of the characteristic tensors of the laminate (in terms of both stiffness and strength).

It is noteworthy that the *blending requirement* (also known as *ply-drop requirement*) is a manufacturing constraint dealing with the continuity of the ply orientation angles between adjacent composite laminates having different thickness. This continuity is essential for the correct junction of laminates having different number of layers. If the formulation of this constraint is immediate and intuitive when the design problem is stated in the space of the layers orientations, this is not true when considering the multi-level approach based on PPs (or, equivalently, the one based on LPs). Specifically, a first formulation of the blending requirement in the PPs space, i.e., regardless of the nature of the stacking sequences of the laminates with different thickness composing the structure, has been introduced in [39], whilst a narrower formulation of the blending constraints has been recently presented in [42]. The latter formulation has been used in this paper.

From a general perspective, the main advantages of the multi-level design approaches (both LPs-based and PPs-based) are essentially two. Firstly, the number of design variables involved in the problem formulation is drastically lower than the one characterising the direct approach. Secondly, the non-convexity characterising the constrained non-linear programming problem (CNLPP) of the FLP is strongly relaxed during the first step (but the feasibility domain of the laminate is still non-convex). As far as the disadvantages are concerned, provided that the splitting of the design problem in FLP and SLP is possible, one of the main issues is to correctly formulate design requirements that intervene at lower scales, like manufacturability constraints and constraints related to the failure of the material, in terms of equivalent constraints to be imposed on the macroscopic design variables involved in the first step. When these conditions are not met, the characteristic scales of the problem cannot be considered as separated and the decomposition of the design problem in FLP and SLP is no longer possible, thus a different approach must be adopted. In such cases, since different physical phenomena occur at multiple scales a sound approach to correctly design composite structures consists in using dedicated global–local (GL) modelling strategies within the optimisation process. GL modelling strategies are generally used when a good balance between accuracy in the assessment of structural responses and low computational effort is sought. Indeed, structural responses involved at lower scales (typically the lamina-level) require refined models, which, however, increase the computational costs.

In the following of this section the focus is put only on the GL modelling strategies developed for the analysis of thin-walled structures typically used in the aerospace field. Indeed, the design and analysis of such structures require a detailed evaluation of the stress field. Nevertheless, the complexity of large structures and the use of composite materials significantly increases the computational costs of the numerical models. Typical finite element (FE) models of aircraft structures in the preliminary design phase are characterised by the combination of 1D and 2D elements, which are appropriately selected to simulate stringers, panels, ribs and other components. This discretisation is, obviously, a simplification of reality, but it is necessary because it allows the designer

to have an idea of the distribution of stresses in the structure, although they are affected by the simplifying assumptions at the basis of the classical theories associated with the 1D/2D elements used by commercial software. However, 3D stress fields should be taken into account when geometric discontinuities of the structure are present, e.g., holes, joints and free edges and, above all, if composite materials are used. To accurately capture these localised 3D stress fields, the classic theories and kinematic models cannot be used for this task and solid models or high-order theories are often necessary. However, using a full 3D FE model or a FE model composed of elements based on high-order kinematic models for a large-size structure is prohibitive in terms of computational effort.

To make the model more efficient, i.e., to find a good balance between computational costs and results accuracy, three main classes of GL modelling are often employed in the literature. The first class of GL modelling strategies is based on a mesh refinement or the shape functions modification within the critical regions of the structure [43–45]. The second class makes use of multi-model methods, wherein different subregions of the structure are analysed with different mathematical models [46–52]. The third class is based on the use of the static condensation technique, also known as "super-elements method" [53], to alleviate the computational effort.

Among the few works making use of a GL modelling strategy in the framework of an optimisation process, one can find the work by Arrieta and Stritz [54], who proposed a GL modelling strategy dedicated to damage tolerance analyses of the structural components of a conventional wing. Of course, this type of analyses requires a refined model of structural components to simulate cracks onset and growth. An alternative approach is presented in [55]. However, the global model does not take stringers and spar-caps into account, since stiffened panels are modelled as equivalent shells. In [56], a GL approach for a high-speed wing is presented. The main limitation of this study is about the remapping of the local models over rectangular plane stiffened plates, loosing in this way the effect of geometrical details on the buckling strength of the structure. Furthermore, in [56], several constraints are evaluated using simplified analytic formulæ. Liu et al. [57] presented a GL modelling approach for the optimisation of curvilinear spars and ribs (SpaRibs). The problem formulation presents a major issue: the procedure needs a significant computational effort (hundreds of cores) to find solutions in acceptable time, loosing in this way the interest behind the GL modelling approach.

Recently, some efforts to formalise and include a GL modelling approach based on the *sub-modelling technique* into the MS2LOS to design large-size composite structures have been carried out by considering both meta-heuristic algorithms[39,40,58–60] and deterministic ones [41,61]. Nevertheless, in all these works, the scales have been considered as separated and the design problem has been split in FLP and SLP according to the classic MS2LOS. The structural responses evaluated at the lower scales have been integrated in the formulation of the FLP through equivalent (conservative) constraints on the PPs of the laminates constituting the structure. However, such an approach, although computationally efficient, leads, sometimes, to conservative solutions that can be still improved, especially when the lightness is the driving criterion of the optimisation process (which is the case for large-size aerospace structures).

To this end, in this work, a modified version of the MS2LOS is proposed and its effectiveness is proven on a simplified wing-box model made of composite materials taken from [39]. The aim is to integrate the global–local approach based on the Carrera's Unified Formulation (CUF) presented in [62] into the MS2LOS. The problem is formulated in terms of the least-weight design of the composite wing-box structure subject to design requirements

related to blending, buckling and first-ply failure. This last requirement is verified by using the global–local modelling approach involving a local layer-wise model based on CUF higher-order beam theories. The critical zone of interest (ZOI) of the wing-box is identified by means of the tensorial laminate-level failure criterion presented in [63,3]. To achieve this task and find an optimal configurations meeting the design requirements at all scales, the work-flow of the MS2LOS has been modified in order to integrate the global–local modelling approach based on CUF and to determine feasible stacking sequences satisfying the requirements of the problem at hand. Particularly, in the framework of the proposed optimisation strategy, there is no longer a clear distinction between FLP and SLP, but the two phases of the MS2LOS strongly interact during the optimisation process. More precisely, at the macroscopic scale the laminate behaviour is still described through the use of PPs, which constitute (together with the geometrical parameters) the design variables of the FLP. The solution search of the FLP is carried out through the EvolutionaRy Algorithm for optimiSation of ModUlar Systems (ERASMUS), a special GA developed by Montemurro [16]. However, since requirements on the first-ply failure index and on the delamination are introduced in the problem formulation and since the most critical ZOI is modelled through a layer-wise FE model, for each individual representing the potential solution of the FLP, a nested genetic optimisation is carried out to find the optimal stack matching the values of the PPs corresponding to this individual and satisfying the requirement on the first-ply failure and delamination at the lower scale. In this context, the optimal stacking sequence, for each individual of the FLP, is searched in the domain of general quasi-trivial (QT) solutions [64,65] without introducing simplifying hypotheses on the stack nature.

The reminder of the paper is as follows. The fundamentals of the polar method are briefly recalled in Section 2 for both stiffness and strength properties, whilst the fundamentals of the CUF are briefly introduced in Section 3. The problem description and the general work-flow of the design procedure are presented in Section 4. The mathematical formulation of the optimisation problem and the numerical strategy are detailed in Section 5. The global FE model of the simplified wing-box and the local 1D CUF model of the ZOI are described in Section 6, while the numerical results are discussed in Section 7. Finally, Section 8 is devoted to concluding remarks and prospects.

Notation. Upper-case bold letters and symbols are used to indicate tensors and matrices, while lower-case bold letters and symbols indicate column vectors.

2. Fundamentals of the polar method

In this section, the fundamentals of the polar method applied to laminates stiffness and strength matrices are briefly recalled; for a deeper insight in the matter, the reader is addressed to previous works [13,14,63,66].

The polar method, introduced by Verchery [12], allows expressing any n-rank plane tensor through a set of tensor invariants, which can be related to specific values of the PPs. In the context of this work, two types of tensors are relevant: second-rank symmetric plane tensors Z_{ij} (with $i,j = 1,2$) and fourth-rank elasticity-like (i.e., having both major and minor symmetries) plane tensors L_{ijkl} (with $i,j,k,l = 1,2$). They can be expressed in terms of their PPs as:

$$
\begin{aligned}
Z_{11} &= +T & +R\cos 2\Phi, \\
Z_{12} &= & +R\sin 2\Phi, \\
Z_{22} &= +T & -R\cos 2\Phi,
\end{aligned}
\tag{1}
$$

and

$$
\begin{aligned}
L_{1111} &= +T_0 & +2T_1 & +R_0\cos 4\Phi_0 & +4R_1\cos 2\Phi_1, \\
L_{1122} &= -T_0 & +2T_1 & -R_0\cos 4\Phi_0, \\
L_{1112} &= & & +R_0\sin 4\Phi_0 & +2R_1\sin 2\Phi_1, \\
L_{2222} &= +T_0 & +2T_1 & +R_0\cos 4\Phi_0 & -4R_1\cos 2\Phi_1, \\
L_{2212} &= & & -R_0\sin 4\Phi_0 & +2R_1\sin 2\Phi_1, \\
L_{1212} &= +T_0 & & -R_0\cos 4\Phi_0.
\end{aligned}
\tag{2}
$$

In Eqs. (1) and (2), T, T_0 and T_1 are the isotropic moduli, R, R_0 and R_1 are the anisotropic ones, while Φ, Φ_0 and Φ_1 are the polar angles. Among them T, R and T_0, T_1, R_0, R_1, $\Phi_0 - \Phi_1$ are tensor invariants, while Φ and one of the two polar angles, Φ_0 or Φ_1, can be arbitrarily chosen to set the reference frame, for second and fourth rank tensors, respectively.

One of the main advantages of the polar formalism is that requirement on elastic symmetries of the tensor can be translated into simple algebraic conditions on the related PPs. For example, the ordinary orthotropy of a fourth-rank elasticity-like tensor corresponds to the condition:

$$
\Phi_0 - \Phi_1 = K\pi/4,
\tag{3}
$$

with $K = 0$ and $K = 1$, corresponding to the so-called low shear modulus and high shear modulus orthotropy, respectively. More details about the elastic symmetries and their expression in terms of PPs can be found in [66].

2.1. Polar parameters of the laminate stiffness matrices

In the framework of the first-order shear deformation theory (FSDT) [67] the constitutive law of the laminate (expressed within the local frame $\Gamma_e = \{O; x_e, y_e, z_e\}$) can be stated as:

$$
\mathbf{r} = \mathbf{K}_{\text{lam}}\boldsymbol{\varepsilon},
\tag{4}
$$

where $\mathbf{r}$ and $\boldsymbol{\varepsilon}$ are the vectors of the generalised forces per unit length and the strains of the laminate middle plane, respectively, whilst $\mathbf{K}_{\text{lam}}$ is the laminate stiffness matrix (in Voigt's notation). In this framework, the analytical form of these arrays is:

$$
\mathbf{r} := \begin{Bmatrix} \mathbf{n} \\ \mathbf{m} \\ \mathbf{q} \end{Bmatrix}, \quad
\mathbf{K}_{\text{lam}} := \begin{bmatrix} \mathbf{A} & \mathbf{B} & \mathbf{0} \\ & \mathbf{D} & \mathbf{0} \\ \text{sym} & & \mathbf{H} \end{bmatrix}, \quad
\boldsymbol{\varepsilon} := \begin{Bmatrix} \boldsymbol{\varepsilon}_0 \\ \boldsymbol{\chi}_0 \\ \boldsymbol{\gamma}_0 \end{Bmatrix}.
\tag{5}
$$

In Eq. (5), $\mathbf{A}$, $\mathbf{B}$ and $\mathbf{D}$ are the membrane, membrane/bending coupling and bending stiffness matrices of the laminate, while $\mathbf{H}$ is the out-of-plane shear stiffness matrix. $\mathbf{n}$, $\mathbf{m}$ and $\mathbf{q}$ are the vectors of membrane forces, bending moments and shear forces per unit length, respectively, whilst $\boldsymbol{\varepsilon}_0$, $\boldsymbol{\chi}_0$ and $\boldsymbol{\gamma}_0$ are the vectors of in-plane strains, curvatures and out-of-plane shear strains of the laminate middle plane, respectively. In order to analyse the elastic response of the multilayer plate, it is useful to introduce the laminate normalised stiffness matrices:

$$
\mathbf{A}^* := \frac{1}{t}\mathbf{A}, \quad \mathbf{B}^* := \frac{2}{t^2}\mathbf{B}, \quad \mathbf{D}^* := \frac{12}{t^3}\mathbf{D}, \quad \mathbf{H}^* := \frac{1}{t}\mathbf{H},
\tag{6}
$$

where t is the total thickness of the laminate.

As deeply discussed by Montemurro [13,14], $\mathbf{A}^*$, $\mathbf{B}^*$, $\mathbf{D}^*$ behave like tensor $\mathbf{L}$ of Eq. (2) and $\mathbf{H}^*$ behaves like tensor $\mathbf{Z}$ of Eq. (1), therefore it is possible to express the Cartesian components of these matrices in terms of PPs, for an overall number of 21 parameters. It can be proven that, if the elastic properties of the constitutive ply (i.e., matrices $\mathbf{Q}^{\text{in}}$ and $\mathbf{Q}^{\text{out}}$ and their PPs, listed in Table 1) are known and the hypothesis of fully orthotropic quasi-homogeneous laminate is introduced, i.e.,

$$
\mathbf{A}^* = \mathbf{D}^*, \quad \mathbf{B}^* = \mathbf{0}, \quad \Phi_0^{\mathbf{A}^*} - \Phi_1^{\mathbf{A}^*} = K^{\mathbf{A}^*}\pi/4,
\tag{7}
$$

the overall number of independent PPs reduces to only three: the anisotropic polar moduli $R_{0K}^{A^*} := (-1)^{K^{A^*}} R_0^{A^*}$ and $R_1^{A^*}$, which describe the type of the orthotropy of matrix $\mathbf{A}^*$, and the polar angle $\Phi_1^{A^*}$, which represents the orientation of the main orthotropy axis of matrix $\mathbf{A}^*$. More details on the polar formalism and its application in the context of the FSDT are available in [13,14].

2.2. Polar parameters of the laminate strength matrices

For the assessment of failure at the laminate level, the general laminate-level failure criterion (FC) formulation introduced by Catapano and Montemurro [63] is here employed. This criterion represents a general unified formula including various phenomenological failure criteria. Particularly, the laminate-level failure will be described through the Tsai-Wu (TW) FC. It is well-known that the ply-level TW FC [68] can be written in matrix notation as

$$F_{TW} := \boldsymbol{\sigma}^T \mathbf{F} \boldsymbol{\sigma} + \boldsymbol{\sigma}^T \mathbf{f} \leqslant 1, \tag{8}$$

where $\boldsymbol{\sigma}$ is the stress vector in Voigt's notation, while $\mathbf{F}$ and $\mathbf{f}$ depend on the lamina strength properties [68]. In agreement with Khani et al. [69], the stress dependent term F_{12} is assumed equal to

$$F_{12} = \frac{-1}{\sqrt{X_t X_c Y_t Y_c}}, \tag{9}$$

where X_α, Y_α ($\alpha = c, t$) are the limit stresses along x and y axes, respectively, listed in Table 1. By introducing the FSDT hypothesis of null out-of-plane normal stress, by separating the in-plane and out-of-plane contributions, by using the Hooke's law and by exploiting the FSDT kinematics, Eq. (8) can be rewritten for each layer k in terms of the laminate middle plane strains

$$F_{TW}^k(z) = \boldsymbol{\varepsilon}_0^T \mathbf{G}_k^{in} \boldsymbol{\varepsilon}_0 + z^2 \boldsymbol{\chi}_0^T \mathbf{G}_k^{in} \boldsymbol{\chi}_0 + 2z \boldsymbol{\varepsilon}_0^T \mathbf{G}_k^{in} \boldsymbol{\chi}_0 \\ + \boldsymbol{\gamma}_0^T \mathbf{G}_k^{out} \boldsymbol{\gamma}_0 + \boldsymbol{\varepsilon}_0^T \mathbf{g}_k^{in} + z \boldsymbol{\chi}_0^T \mathbf{g}_k^{in} \leqslant 1, \tag{10}$$

where the matrices $\mathbf{G}_k^{in}, \mathbf{G}_k^{out}$ and the vector $\mathbf{g}_k^{in}$ depend on the strength properties of the ply (listed in Table 1) and on the orientation of the k-th layer.

The *laminate failure index* (LFI) is calculated by averaging Eq. (10) through the thickness t of the laminate as:

$$F_{TW}^{lam} = \frac{1}{t} \int_{-t/2}^{t/2} F_{TW}^k(z) \, dz. \tag{11}$$

Eq. (11) simplifies to:

$$F_{TW}^{lam} = \frac{1}{t} \left(\boldsymbol{\varepsilon}_0^T \mathbf{G}_A \boldsymbol{\varepsilon}_0 + \boldsymbol{\chi}_0^T \mathbf{G}_D \boldsymbol{\chi}_0 + \boldsymbol{\varepsilon}_0^T \mathbf{G}_B \boldsymbol{\chi}_0 \\ + \boldsymbol{\gamma}_0^T \mathbf{G}_H \boldsymbol{\gamma}_0 + \boldsymbol{\varepsilon}_0^T \mathbf{g}_A + \boldsymbol{\chi}_0^T \mathbf{g}_D \right). \tag{12}$$

Matrices $\mathbf{G}_A, \mathbf{G}_B, \mathbf{G}_D$ and $\mathbf{G}_H$ and vectors $\mathbf{g}_A$ and $\mathbf{g}_D$ represent the laminate strength matrices and vectors. In particular, the four matrices can be seen as the strength counterpart of stiffness matrices $\mathbf{A}, \mathbf{B}, \mathbf{D}$, and $\mathbf{H}$. The laminate normalised strength matrices and vectors can be defined as follows:

$$\mathbf{G}_A^* = \frac{1}{t} \mathbf{G}_A, \quad \mathbf{G}_B^* = \frac{2}{t^2} \mathbf{G}_B, \quad \mathbf{G}_D^* = \frac{12}{t^3} \mathbf{G}_D, \quad \mathbf{G}_H^* = \frac{1}{t} \mathbf{G}_H, \\ \mathbf{g}_A^* = \frac{1}{t} \mathbf{g}_A, \quad \mathbf{g}_D^* = \frac{2}{t^2} \mathbf{g}_D. \tag{13}$$

Finally, by defining

$$\mathbf{G}_{lam} := \begin{bmatrix} \mathbf{G}_A & \mathbf{G}_B & \mathbf{0} \\ & \mathbf{G}_D & \mathbf{0} \\ \text{sym} & & \mathbf{G}_H \end{bmatrix}, \quad \mathbf{g}_{lam} := \begin{Bmatrix} \mathbf{g}_A \\ \mathbf{g}_D \\ \mathbf{0} \end{Bmatrix}, \tag{14}$$

a compact version of Eq. (12) can be obtained:

$$F_{TW}^{lam} = \boldsymbol{\varepsilon}^T \frac{\mathbf{G}_{lam}}{t} \boldsymbol{\varepsilon} + \boldsymbol{\varepsilon}^T \frac{\mathbf{g}_{lam}}{t}. \tag{15}$$

To use the LFI, a suitable threshold value F_{th} must be introduced, such that, when failure occurs

$$F_{TW}^{lam} \geqslant F_{th}. \tag{16}$$

A thorough discussion about the choice of F_{Th}, which is not the main scope of this work, is reported in [4].

Of course, the arrays of Eq. (14) can be expressed in terms of PPs. Catapano and Montemurro [63] showed that, when the strength properties of the constitutive ply (i.e., matrices $\mathbf{G}^{in}$ and $\mathbf{G}^{out}$ and vector $\mathbf{g}^{in}$, and their PPs, listed in Table 1) are known, the laminate strength matrices and vectors can be expressed in terms of the PPs of the laminate stiffness matrices introduced in Section 2.1. This means that the PPs describing the laminate stiffness and strength matrices and vectors are not independent. Accordingly, it suffices to include among the problem design variables only one of these two sets of PPs. When a fully-orthotropic quasi-homogeneous laminate is considered, the overall number of independent PPs describing its behaviour (in terms of both stiffness and strength) is still equal to three: the anisotropic polar moduli $R_{0K}^{A^*}$ and $R_1^{A^*}$ and the polar angle $\Phi_1^{A^*}$ of matrix $\mathbf{A}^*$ or, alterna-

Table 1
Mechanical properties of the T300/5208 carbon-epoxy pre-preg used in this study.

Technical constants		PPs of $\mathbf{Q}_{in}$[a]		PPs of $\mathbf{Q}_{out}$[b]	
E_1 [MPa]	142000.0	T_0 [MPa]	22040.0	T [MPa]	5272.0
E_2 [MPa]	10300.0	T_1 [MPa]	19838.0	R [MPa]	1928.0
G_{12} [MPa]	7200.0	R_0 [MPa]	14840.0	Φ [deg]	90.0
ν_{12}	0.27	R_1 [MPa]	16550.0		
ν_{23}	0.42	Φ_0 [deg]	0.0		
		Φ_1 [deg]	0.0		
Engineering strengths		PPs of $\mathbf{G}_{in}$[c]		PPs of $\mathbf{G}_{out}$[d] and $\mathbf{g}_{in}$[e]	
X_t [MPa]	2280.0	Γ_0 [MPa]	7077.0	Γ [MPa]	8637
X_c [MPa]	1440.0	Γ_1 [MPa]	1312.0	Λ [MPa]	1647.0
Y_t [MPa]	57.0	Λ_0 [MPa]	3206.0	Ω [deg]	90.0
Y_c [MPa]	228.0	Λ_1 [MPa]	405.0		
Z_c [MPa]	57.0	Ω_0 [deg]	45.0	γ [MPa]	68.0
S_{23} [MPa]	40.0	Ω_1 [deg]	90.0	λ [MPa]	68.0
$S_{12} = S_{13}$ [MPa]	71.0	θ [MPa]	90.0		
Thickness:				$t_{ply} = 0.127$ [mm]	
Density:				$\rho_{ply} = 1.578 \times 10^{-6}$ [kg/mm³]	

[a] In-plane reduced stiffness matrix.
[b] Out-of-plane shear stiffness matrix.
[c] In-plane reduced strength matrix.
[d] Out-of-plane strength matrix.
[e] In-plane strength vector.

tively, their counterpart of matrix $\mathbf{G}_A^*$. More details on the representation of the strength matrices of the laminate through the polar formalism and on the correlation between the PPs of strength and stiffness matrices of the laminate can be found in [63].

3. 1D finite element model based on the unified formulation

In this section, the fundamentals of the Carrera's unified formulation (CUF) are briefly recalled for beam-like structures for a fruitful understanding of the global/local modelling strategy described in Section 6. For a deeper insight in the matter, the reader is addressed to [70]. Consider a generic beam whose longitudinal axis coincides with the y axis and its cross-section lies on the xz-plane, as shown in Fig. 1. Let $\mathbf{u}^T(x,y,z) = \{u_x(x,y,z), u_y(x,y,z), u_z(x,y,z)\}$ be the displacement vector at the generic point of the beam. The cross-section of the structure is denoted by Ω, and the coordinate y along the beam axis takes value in the interval $[0, L]$. In the following, the strain tensor $\boldsymbol{\varepsilon}$ and the stress tensor $\boldsymbol{\sigma}$ are expressed according to the Voigt's notation. In the case of small displacements, the strain - displacement relationship can be written in compact form as:

$$\boldsymbol{\varepsilon} = \mathscr{D}\mathbf{u}, \tag{17}$$

where $\mathscr{D}$ is the linear differential operator. The stress tensor components can be assessed through the Hooke's law:

$$\boldsymbol{\sigma} = \mathbf{C}\boldsymbol{\varepsilon}, \tag{18}$$

where $\mathbf{C}$ is the stiffness matrix of the material. For the sake of brevity, matrices $\mathscr{D}$ and $\mathbf{C}$ are not reported here, but their expression can be found in [70]. In the framework of the CUF [70], the displacement field over the cross-section can be expressed as follows:

$$\mathbf{u}(x,y,z) = F_\tau(x,z)\mathbf{u}_\tau(y), \qquad \tau = 1, 2, \ldots, M, \tag{19}$$

where each function F_τ varies over the cross-section, $\mathbf{u}_\tau$ is the generalised displacement vector and M stands for the number of terms of the expansion (note that the repeated subscript τ indicates summation). Of course, the choice of F_τ determines the class of the 1D CUF model. In this paper, F_τ are Lagrange Expansions (LE) which are based on the use of Lagrange polynomials as generic functions to describe the displacement field variation over the cross-section. The cross-section is divided into local expansion sub-domains, whose polynomial degree depends on the type of LE employed. Three-node linear L3, four-node bilinear L4, nine-node cubic L9, and sixteen-node quartic L16 polynomials can be used to formulate refined beam theories [70]. Of course, LE allows for taking into account arbitrary section geometries. The locations of the points belonging to a generic L9 sub-domain, in terms of natural coordinates, are listed in Table 2. In the case of an L9 element, the interpolation functions are given by:

$$F_\tau = \frac{1}{4}(\alpha^2 + \alpha\alpha_\tau)(\beta^2 + \beta\beta_\tau), \qquad \tau = 1, 3, 5, 7,$$
$$F_\tau = \frac{1}{2}\beta_\tau^2(\beta^2 + \beta\beta_\tau)(1 - \alpha^2) + \frac{1}{2}\alpha_\tau^2(\alpha^2 + \alpha\alpha_\tau)(1 - \beta^2), \qquad \tau = 2, 4, 6, 8,$$
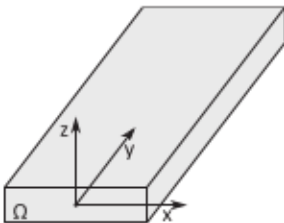$$F_\tau = (1 - \alpha^2)(1 - \beta^2), \qquad \tau = 9,$$

Fig. 1. Coordinate frame of the beam model.

where α, $\beta \in [-1, 1]$. In the case of L9 polynomials, the displacement field reads:

$$u_x = F_1 u_{x1} + F_2 u_{x2} + F_3 u_{x3} + F_4 u_{x4} + F_5 u_{x5} + F_6 u_{x6} + F_7 u_{x7} + F_8 u_{x8} + F_9 u_{x9},$$
$$u_y = F_1 u_{y1} + F_2 u_{y2} + F_3 u_{y3} + F_4 u_{y4} + F_5 u_{y5} + F_6 u_{y6} + F_7 u_{y7} + F_8 u_{y8} + F_9 u_{y9},$$
$$u_z = F_1 u_{z1} + F_2 u_{z2} + F_3 u_{z3} + F_4 u_{z4} + F_5 u_{z5} + F_6 u_{z6} + F_7 u_{z7} + F_8 u_{z8} + F_9 u_{z9}.$$

Refined beam models can be obtained by adopting high-order Lagrange polynomials or by using a combination of Lagrange polynomials on multi-domain cross-sections. More details about high-order models based on LE can be found in [70,71].

Thanks to the multi-domain nature of the LE-based models, *layer - wise* models can be implemented straightforwardly by considering one or more local expansions for each layer of the composite structure. Of course, the beam is meshed along the y-axis according to the classical FE method. Particularly, the generalised displacement vector $\mathbf{u}_\tau(y)$ is approximated through classic shape functions $N_i(y)$ as follows:

$$\mathbf{u}(x,y,z) = N_i(y)F_\tau(x,z)\mathbf{u}_{i\tau}, \qquad \tau = 1, \ldots, M, \qquad i = 1, \ldots, n_n, \tag{20}$$

where $N_i(y)$ is the i-th shape function, n_n is the number of nodes in one element and $\mathbf{u}_{i\tau}$ is the vector of nodal unknowns. For the sake of brevity, the shape functions are not reported here, but can be found in classical books, like [43]. Elements with four nodes (B4) are adopted in this work, in this way a cubic approximation along the y-axis is assumed. The correspondent virtual variation of the displacement can be written as:

$$\delta\mathbf{u}(x,y,z) = N_j(y)F_s(x,z)\delta\mathbf{u}_{js}, \qquad s = 1, \ldots, M, \qquad j = 1, \ldots, n_n. \tag{21}$$

The governing equations are derived by applying the principle of virtual displacements (PVD). For a static problem:

$$\delta L_{int} = \delta L_{ext}, \tag{22}$$

where δL_{int} is the virtual variation of the internal work, δL_{ext} is the virtual variation of work done by the external loads. The virtual variation of the internal work can be expressed as:

$$\delta L_{int} = \int_V \delta\boldsymbol{\epsilon}^T\boldsymbol{\sigma}dV. \tag{23}$$

By using Eqs. (17), (18) and (20) the previous expression simplifies to:

$$\delta L_{int} = \delta\mathbf{u}_{js}^T\mathbf{K}^{ij\tau s}\mathbf{u}_{i\tau}, \tag{24}$$

where $V = \Omega L$ is the volume of the beam and $\mathbf{K}^{ij\tau s}$ is the stiffness matrix in the form of a 3×3 fundamental nucleus (FN). The derivation of the FN can be found in [71]. It is noteworthy that the formal expression of the components of the FN of the stiffness matrix does not depend on the choice of the cross-sectional functions F_τ, which are related to the theoretical model at the basis of the element. Moreover, it is not influenced by the choice of the shape functions N_i, which determine the numerical accuracy of the FE model approximation. This means that any classical or high-order beam element can be automatically formulated by opportunely expanding the FN according to the indices τ, s, i, and j. The formal expression of the load vector coherent to the considered model and theory can be found in [70].

4. Problem Description

4.1. The benchmark structure

The benchmark structure considered here is a simplified wing-box model made of composite laminates. The geometry of the

Table 2
Natural coordinates of the points belonging to an L9 cross-section element.

| Point	α_τ	β_τ
1	−1	−1
2	0	−1
3	+1	−1
4	+1	0
5	+1	+1
6	0	+1
7	−1	+1
8	−1	0
9	0	0

structure, taken from [39], the boundary conditions (BCs) and the applied loads are illustrated in Fig. 2. The wing-box has a length $L = 3543$ mm, a width $W = 2240$ mm and a height $H = 381$ mm. The wing-box is clamped at $x = 0$ and four concentrated forces are applied at nodes located at $(x, y, z) = (L, i\frac{W}{3}, \frac{H}{2}), i = 0,3$. The magnitudes of the forces are $F_1 = 360.04$ N, $F_2 = 751.55$ N, $F_3 = 751.55$ N and $F_4 = 1520.70$ N.

In the simplified wing-box, ribs, spars and stringers are replaced by continuous equally spaced composite plates with a pre-defined stacking sequence, i.e., $[45°_{11}]_S$. All laminates are made of T300/N5208 graphite-epoxy pre-preg laminæ whose mechanical properties are reported in Table 1.

In this study, only dorsal and ventral panels are optimised. Conversely, the laminates constituting ribs, spars and stringers are kept unchanged during the optimisation process. For the sake of clarity, Fig. 3 shows the design and non-design regions of the wing box. The design region consists of six panels: three belonging to the dorsal region and three belonging to the ventral one. Moreover, the following hypothesis is introduced on the macroscopic behaviour of each panel composing the design region: it behaves as a fully orthotropic quasi-homogeneous laminate, for which Eq. (7) holds.

$u_x = u_y = u_z = 0$
$\theta_x = \theta_y = \theta_z = 0$
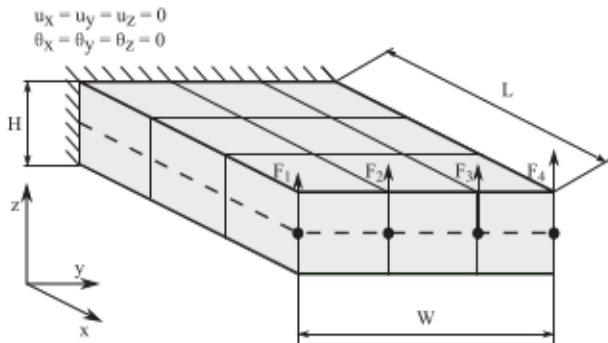
Fig. 2. Geometry and BCs of the simplified wing-box taken from [39].
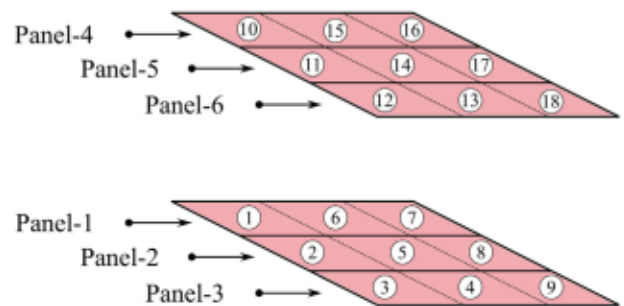

Design Region
Non-Design Region
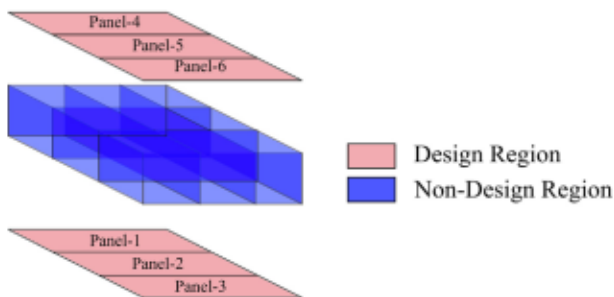
Fig. 3. Design and non-design regions of the wing-box structure.

Two types of FE models will be used during the optimisation process: (i) the global finite element model (GFEM) wherein the mechanical response of each laminate belonging to the design region is described in terms of PPs (in the FSDT framework) regardless of the stacking sequence nature; (ii) the local finite element model (LFEM), made of 1D high-order four-node beam elements (B4) belonging to the LE class (layer-wise kinematics), which is generated only for the most critical ZOI within the design region [72]. Particularly, as illustrated in Fig. 4, each panel of the design region is split into three sub-panels to check the design requirements related to the LFEM generated for the most critical ZOI. All the results presented in this study are compared to the ones obtained for a reference configuration of the wing-box. More precisely, the design region of the reference solution is composed of quasi-homogeneous isotropic laminates with a number of plies equal to 20: the total mass of the reference solution is, thus, $M_{ref} = 261$ kg.

4.2. The standard multi-scale two-level optimisation strategy

In the context of the classical MS2LOS based on PPs, introduced in [33,34] and used in different real-world engineering problems [1–5,37–42,61,73], the optimisation problem is split into the following two distinct (but related) optimisation problems.

- **First-level problem (FLP).** The aim of this phase (which focuses on the macroscopic scale) is the determination of the optimal value of both PPs and geometric parameters of the laminates composing the structure to satisfy the requirements of the problem at hand, which is formulated as a constrained non-linear programming problem (CNLPP). At this level, each laminate is modelled as an equivalent homogeneous anisotropic plate whose behaviour is described in terms of the laminate PPs (see Section 2). The CNLPP formulation can include design requirements of different nature, e.g., stiffness, buckling factor, eigen-frequencies, technological constraints, etc., formulated in the space of the PPs and of the geometric variables of the composite structure. As discussed in the works available in the literature on this topic, the FLP can be solved either by means of a deterministic algorithm [1,4,5,41,42,61] (in this case the analytical form of the gradient of each design requirement must be provided to speed-up the calculation) or through a metaheuristic algorithm [2,3,38,37,39,40,73].
- **Second-level problem (SLP).** The SLP, which is formulated at the laminate mesoscopic scale (i.e., the ply-level), is devoted to the determination of a suitable lay-up matching the optimum values of the PPs resulting from the FLP. In the case of constant stiffness composite structures, the design variables are the orientation angles of the layers [33,34,37], whilst in the case of the variable stiffness composite structures, the unknowns are the

Fig. 4. Sub-panels composing the design region of the wing-box.

parameters describing the fibres-paths within each lamina [2,3,73]. The SLP is usually formulated as an unconstrained non-linear programming problem (UNLPP) [34].

4.3. The modified multi-scale two-level optimisation strategy

The aim of this study is to integrate the global–local modelling approach based, on the one hand, on a standard FE code to generate the GFEM (to assess the global structural responses) and, on the other hand, on high-order layer-wise beam theories in the framework of CUF (to assess local design requirements) in the MS2LOS for composite structures. As discussed in the following, the overall structure of the MS2LOS must be properly modified to achieve this task.

The main reason is to accurately assess the local structural responses through the use of high-order theories to better characterise the mechanical behaviour of the most critical ZOI of the FE model overcoming, thus, the limitations of the FSDT on which the GFEM relies. The work-flow of the modified MS2LOS is illustrated in Fig. 5.

Regarding the benchmark structure illustrated in Fig. 2, the goal is to minimise the mass of the structure subject to the following design requirements: buckling factor (evaluated through the GFEM), feasibility constraints on PPs of the laminates composing the wing-box, blending constraints between adjacent panels [39,41], first-ply failure on the most critical ZOI (evaluated through the LFEM).

As illustrated in Fig. 5, the modified architecture of the MS2LOS is composed of two nested optimisation loops. The solution search for both loops is performed through the GA ERASMUS [16]. The outer loop represents the structural optimisation, i.e., the FLP, where both GFEM (built within ANSYS®) and LFEM (generated within the CUF framework) are interfaced with ERASMUS. The inner loop represents the lay-up design of the SLP (this step is fully analytical, see Section 5), which is performed only for the most critical ZOI of the design region of the wing-box (the stacking sequences related to the other panels can be determined through the efficient and general strategy discussed in [42]). Specifically, during the outer loop, for each individual of each population, ERASMUS passes the vector of design variables $\mathbf{x}_{out}$ (see Section 5 for more details) to the GFEM, which is invoked to assess the mass of the wing-box, the first buckling factor, the blending constraints according to the formulation proposed in [42], and the LFI according to the formulation proposed by Catapano and Montemurro [3,63]. The LFI is then used to identify the most critical ZOI among the sub-panels constituting the design region of the wing-box, as shown in Fig. 4. It is noteworthy that the GFEM is generated by considering the definition of the laminates (constituting the wing-box) based on the PPs in the FSDT framework (thus the stacking sequence is not defined within the GFEM). Once the most critical panel of the wing-box is identified, the SLP is resolved on-the-fly to find, at least, one optimal stack meeting the current value of PPs and thickness (included in the vector of design variables $\mathbf{x}_{out}$) for the selected ZOI. It must be noticed that the stacking sequences solutions of the SLP are searched in the space of quasi-trivial (QT) solutions, as discussed in Section 5. Once the near-optimal stack is found, it is passed to the LFEM based on layer-wise high-order beam theories to assess the ply failure index (the CUF environment is invoked to achieve this task). Finally, all requirements (from both GFEM and LFEM) are passed to ERASMUS (outer loop) to perform the genetic operations (selection, crossover, mutation, penalisation, elitism, etc.) until the convergence criterion is met.

According to the work-flow shown in Fig. 5, from an optimisation standpoint, there is a strong coupling between the two loops: the solution of the inner loop (the stack of the ZOI) depends on the current values of the design variables of the outer loop (i.e., PPs and

thickness), whilst the solution of the outer loop implicitly depends upon the solution of the inner loop because the requirement on the first-ply failure is introduced in the problem formulation of the outer loop and is checked on the stacking sequence of the ZOI by means of a refined FE model based on high-order beam theories.

5. Problem formulation

This Section is devoted to the description of the problem formulation by highlighting the main features (design variables, objective function, optimisation constraints) of both outer and inner loops of the process illustrated in Fig. 5.

5.1. Design variables of the outer optimisation loop

The outer optimisation loop focuses on the structural optimisation by considering the structural responses assessed through both GFEM and LFEM. Inasmuch as the local response of the structure, assessed by means of the LFEM, depends upon the macroscopic behaviour of the most critical ZOI extracted from the GFEM (this task is done via the evaluation of the LFI, as discussed in the following), and since the elastic and strength behaviours of the laminates composing the GFEM are described in the PPs space [38,40], the design variables of the outer loop are the laminate PPs $R_{0K}^{A^*}, R_1^{A^*}$ and $\Phi_1^{A^*}$ and two geometric parameters, i.e., overall thickness t and number of saturated groups n_g of the QT solutions, as discussed in the following.

For optimisation purposes, it is useful to consider the dimensionless quantities defined as follows:

$$n := \frac{t}{t_{ply}}, \quad \rho_0 := \frac{R_{0K}^{A^*}}{R_0}, \quad \rho_1 := \frac{R_1^{A^*}}{R_1}, \quad \phi_1 := \frac{\Phi_1^{A^*}}{\pi/2}, \quad (25)$$

where n is the number of layers, t_{ply} is the thickness of the lamina, whilst R_0 and R_1 are the PPs of the in-plane reduced stiffness matrix of the ply listed in Table 1. Particularly, the laminates composing the design region of the wing-box are quasi-homogeneous and fully-orthotropic (both membrane and bending stiffness tensors). Accordingly, as discussed in Section 2, in the FSDT framework, the macroscopic response of a quasi-homogeneous orthotropic laminate is uniquely described by three dimensionless PPs: ρ_0, ρ_1, ϕ_1. Moreover, the main direction of the orthotropy axis is assumed aligned with the x-axis of the wing-bow structure (see Fig. 2): accordingly, $\phi_1 = 0$ for each panel.

In order to ensure that a feasible stacking sequence, matching the optimal PPs resulting from the FLP, could be found as a result of the SLP, the geometrical feasibility conditions proposed by Vannucci [74] must be considered in the FLP. For a quasi-homogeneous orthotropic laminate, these constraints read[1]:

$$\begin{cases} -1 \leqslant \rho_0 \leqslant 1, \\ 0 \leqslant \rho_1 \leqslant 1, \\ 2(\rho_1)^2 - 1 - \rho_0 \leqslant 0. \end{cases} \quad (26)$$

In previous works dealing with optimisation of composite structures making use of PPs [1,2,38,40,41,73,75,76], the above conditions were introduced as explicit constraints into the FLP formulation of the standard MS2LOS. Unlike the aforementioned works, the variable change proposed by Izzi et al. [4] is used here to avoid the introduction of the feasibility constraint on the PPs, i.e., the third formula in Eq. (26), within the problem formulation.

---

[1] These conditions describe the convex-hull of the true feasibility domain, as recently discussed by Picchi Scardaoni and Montemurro in [31], and are valid under the hypothesis that the laminate is composed of a sufficient number of plies, whose orientation angles can get value in a sufficiently big and scattered set.
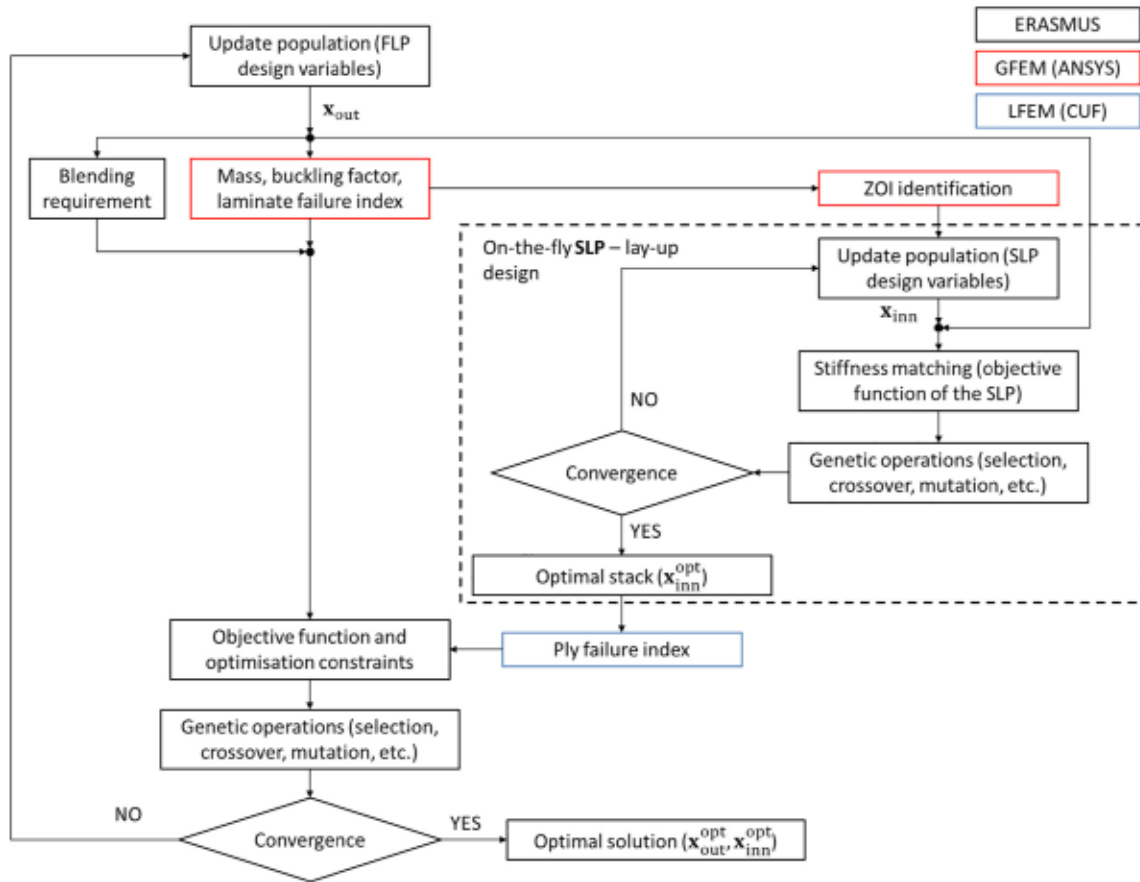
Fig. 5. Work-flow of the modified MS2LOS.

This approach consists of remapping the feasible domain of PPs identified by Eq. (26) over the unit square $[0, 1] \times [0, 1]$ through the following variables change:

$$\alpha_0 := \frac{\rho_0 - 1}{2(\rho_1^2 - 1)}, \quad \alpha_1 := \rho_1, \tag{27}$$

whose converse relations are

$$\rho_0 = 1 + 2\alpha_0 \left(\alpha_1^2 - 1\right), \quad \rho_1 = \alpha_1. \tag{28}$$

In this way, all the combinations of α_0 and α_1 automatically satisfy the feasibility conditions of Eq. (26), without the need of introducing explicit constraints into the problem formulation.

Two geometric parameters complete the set of design variables of the outer optimisation loop: the number of layers n and the number of saturated groups n_g for all the panels of the design regions. The number of layers n is needed to calculate the overall thickness of the laminate t according to Eq. (25), whilst the number of saturated group n_g is used within the inner optimisation loop (i.e., the on-the-fly resolution of the SLP for the most critical ZOI) to correctly select the family of QT solutions within the database generated via the algorithm described in [64]. Indeed, as explained in [64], the number of QT stacks depends upon the combination of n and n_g.

The design variables of the outer optimisation loop are, thus, collected in the following vector:

$$\mathbf{x}_{\text{out}}^{\mathsf{T}} := (\alpha_{0i}, \alpha_{1i}, n_i, n_{gi}), \quad i = 1, \ldots, n_p, \tag{29}$$

where n_p represents the number of panels composing the design region of Fig. 3; accordingly, the overall number of design variables of the outer loop is $n_{\text{out}} = 4n_p$ ($n_p = 6$ in this work).

5.2. Design variables of the inner optimisation loop

As discussed above, the inner optimisation loop, shown in Fig. 5, consists in solving on-the-fly the SLP by searching the solution in the database of QT stacks [64]. As discussed in [64], QT stacks are closed-form solutions that satisfy the requirements of membrane/bending uncoupling and homogeneity (membrane and bending normalised stiffness tensors are equal), regardless of the values of the orientation angles of the layers. Therefore, by means of a dedicated algorithm [64], it is possible to generate the database of QT solutions for a given pair of number of layers n and number of saturated groups n_g. This database was already available at the I2M laboratory as a result of the work by Garulli et al. [64].

Inasmuch as the number of QT solutions n_{QT} depends on the couple n, n_g, i.e., $n_{\text{QT}} = n_{\text{QT}}(n, n_g)$ it is useful to introduce a design variable related to the identifier ID_{QT} (i.e., an integer) that varies in the range $[1, n_{\text{QT}}(n, n_g)]$, which uniquely identifies the solution within the database for a given pair of number of layers and number of saturated groups. Moreover, the orientation angle associated to each saturated group, i.e., $\theta_k, k = 1, \ldots, n_g$ is also included within the design variables vector of the inner loop that reads:

$$\mathbf{x}_{\text{inn}}^{\mathsf{T}} := (\text{ID}_{\text{QT}}, \ \theta_1, \ldots, \ \theta_{n_g}). \tag{30}$$

For a deeper insight in the properties of QT stacks, the reader is addressed to [64].

5.3. Objective function of the inner optimisation loop

The aim of the inner optimisation loop is the lay-up design of each laminate belonging to the design region of the benchmark

structure. The goal is to determine at least one stacking sequence satisfying the values of both geometric parameters and PPs associated to the current individual (of the generic population) of the outer loop resulting from the first level of the strategy and having the elastic symmetries imposed to the laminate at the macroscopic scale, i.e., quasi-homogeneity and orthotropy. In the framework of the FSDT based on the polar formalism for representing the laminate stiffness matrices, the stacking sequence recovery problem, i.e., the SLP, can be stated in the form of an unconstrained optimisation problem (UNLPP) [13,14] as:

$$\min_{\mathbf{x}_{inn}} \quad I(f_i(\mathbf{x}_{inn})), \tag{31}$$

with

$$I(f_i(\mathbf{x}_{inn})) = \sum_{i=1}^{6} f_i(\mathbf{x}_{inn}), \tag{32}$$

where $f_i(\mathbf{x}_{inn})$ are quadratic functions in the space of PPs, each one representing a requirement to be satisfied, like orthotropy, uncoupling, etc. For the problem at hand, the partial objective functions are:

$$f_1(\mathbf{x}_{inn}) = \left(\frac{\Phi_0^{A^*}(\mathbf{x}_{inn}) - \Phi_1^{A^*}(\mathbf{x}_{inn})}{\pi/4} - \tilde{K}^{A^*} \right)^2, \ f_2(\mathbf{x}_{inn}) = \left(\frac{R_0^{A^*}(\mathbf{x}_{inn}) - \tilde{R}_0^{A^*}}{R_0} \right)^2,$$

$$f_3(\mathbf{x}_{inn}) = \left(\frac{R_1^{A^*}(\mathbf{x}_{inn}) - \tilde{R}_1^{A^*}}{R_1} \right)^2, \ f_4(\mathbf{x}_{inn}) = \left(\frac{\Phi_1^{A^*}(\mathbf{x}_{inn}) - \tilde{\Phi}_1^{A^*}}{\pi/4} \right)^2,$$

$$f_5(\mathbf{x}_{inn}) = \left(\frac{\|C(\mathbf{x}_{inn})\|}{\|Q_m\|} \right)^2, \ f_6(\mathbf{x}_{inn}) = \left(\frac{\|B^*(\mathbf{x}_{inn})\|}{\|Q_m\|} \right)^2,$$

$$\tag{33}$$

where $f_1(\mathbf{x}_{inn})$ represents the elastic requirement on the orthotropy of the laminate having the prescribed shape (imposed by the value of $\tilde{K}^{A^*} = 0, 1$ which is related to the sign of ρ_0 of the current individual of the outer optimisation loop), $f_2(\mathbf{x}_{inn})$, $f_3(\mathbf{x}_{inn})$ and $f_4(\mathbf{x}_{inn})$ are the requirements related to the prescribed values of the PPs, i.e., $\tilde{R}_0^{A^*}, \tilde{R}_1^{A^*}, \tilde{\Phi}_1^{A^*} = 0, \tilde{K}^{A^*} = 0, 1$, related to the current individual of the outer optimisation loop, while $f_5(\mathbf{x}_{inn})$ and $f_6(\mathbf{x}_{inn})$ are linked to the quasi-homogeneity condition.

As one can notice from Fig. 5, the SLP must be solved on-the-fly, for each individual of each population of the outer loop. Of course, since the solution search of the SLP is carried out in the space of QT stacks, the terms $f_5(\mathbf{x}_{inn})$ and $f_6(\mathbf{x}_{inn})$ in Eq. (33) are identically null. For more details on the properties of the SLP, the interested reader is addressed to [13,14,37].

The GA ERASMUS is used to perform the solution search of problem (31). The genotype of the individual of the inner loop depends upon the value of the number of saturated groups n_g related to the current individual of the outer loop. In particular, the genotype of the generic individual of the inner optimisation loop is characterised by $n_g + 1$ genes: the first one codes the solution identifier ID$_{QT}$, whilst the remaining ones code the orientation angles of the n_g saturated groups. Each angle can take values in the interval $[-89, 90]$ deg with a step of 1 deg.

5.4. Objective function and optimisation constraints of the outer optimisation loop

The goal of the optimisation process illustrated in Fig. 5 is to minimise the mass of the wing-box, which is, thus, the merit function of the problem at hand. The mass of the wing-box reads:

$$M(\mathbf{x}_{out}) := \rho_{ply} V(\mathbf{x}_{out}), \tag{34}$$

where $V(\mathbf{x}_{out})$ is the overall volume of the GFEM of the wing-box.

The first design requirement, to be included in the problem formulation, consists of a constraint on the first buckling factor λ of the structure. The constraint function reads:

$$g_1(\mathbf{x}_{out}) := 1 - \lambda, \tag{35}$$

where the first buckling factor λ is the result of an eigenvalue buckling analysis conducted on the GFEM of the structure, i.e.,

$$[\mathbf{K}_G(\mathbf{x}_{out}) + \lambda(\mathbf{x}_{out})\mathbf{K}_{\sigma G}(\mathbf{x}_{out})]\psi_G(\mathbf{x}_{out}) = \mathbf{0}. \tag{36}$$

In the above formula, $\mathbf{K}_G(\mathbf{x}_{out})$ and $\mathbf{K}_{\sigma G}(\mathbf{x}_{out})$ are the stiffness and the geometric stiffness matrix of the GFEM, respectively, while $\psi_G(\mathbf{x}_{out})$ is the eigenvector related to the first buckling factor $\lambda(\mathbf{x}_{out})$.

The second and third design requirements deal with the first-ply failure and delamination, respectively, which are assessed by checking a set of inequalities after carrying out a static analysis on the LFEM of the most critical ZOI. As discussed in Section 6, the most critical ZOI is identified and isolated by checking the local LFI calculated from the laminate-level failure criterion presented in Section 2. Once the most critical ZOI is identified, the LFEM is generated by using a high-order beam theory with a layer-wise kinematics in the CUF framework.

Specifically, as discussed in Section 6, the LFEM is subjected to BCs of the Dirichlet type, which are calculated from the results of a static analysis conducted on the GFEM (and opportunely transferred to the LFEM) as follows:

$$\mathbf{K}_G(\mathbf{x}_{out})\mathbf{u}_G(\mathbf{x}_{out}) = \mathbf{f}_G, \tag{37}$$

$$\mathbf{K}_L(\mathbf{x}_{inn})\mathbf{u}_L(\mathbf{x}_{out}, \mathbf{x}_{inn}) + \tilde{\mathbf{K}}_L(\mathbf{x}_{inn})\tilde{\mathbf{u}}_L(\mathbf{x}_{out}) = \mathbf{0}, \tag{38}$$

with

$$\tilde{\mathbf{u}}_L(\mathbf{x}_{out}) := \mathbf{P}\mathbf{u}_G(\mathbf{x}_{out}). \tag{39}$$

In Eq. (37), $\mathbf{u}_G(\mathbf{x}_{out})$ and $\mathbf{f}_G$ are the vectors of generalised displacements and external forces, respectively, of the GFEM. In Eq. (38), $\mathbf{u}_L(\mathbf{x}_{out}, \mathbf{x}_{inn})$ and $\tilde{\mathbf{u}}_L(\mathbf{x}_{out})$ are the unknown and imposed generalised displacements of the LFEM, respectively, whilst matrices $\mathbf{K}_L(\mathbf{x}_{inn})$ and $\tilde{\mathbf{K}}_L(\mathbf{x}_{inn})$ are the stiffness matrices of the LFEM after the application of the BCs of the Dirichlet type.

As stated above, the BCs applied to the LFEM in terms of generalised displacements $\tilde{\mathbf{u}}_L(\mathbf{x}_{out})$ on the LFEM boundary depend upon the results of a static analysis, i.e., the vector $\mathbf{u}_G(\mathbf{x}_{out})$, conducted on the GFEM. The matrix $\mathbf{P}$ of Eq. (39) represents such transformation.

Once the results of the static analysis carried out on the LFEM are available, the first-ply failure is evaluated by using the Hashin's failure criteria for the prediction of ply failure [77] together with the mixed mode quadratic criteria to determine the onset of delamination [78]. All failure criteria considered in this study are assessed at the ply-level by considering the material coordinate system shown in Fig. 6. For the sake of clarity, the Hashin's failure criteria and the delamination criterion used in the formulation of the optimisation problem are briefly described here below.

- Hashin's failure criteria. This set of criteria is used to determine the first-ply failure based on the stress state and to determine the dominating failure mode at the ply-level. The inequalities to be checked (and corresponding to different failure modes for both fibre and matrix) are:
  1. Fibre Tension:
$$g_2(\mathbf{x}_{inn}) := \left(\frac{\sigma_{11}^2}{X_T} \right)^2 + \frac{\sigma_{12}^2 + \sigma_{13}^2}{S_{13}^2} - 1, \tag{40}$$
  2. Fibre Compression:
$$g_3(\mathbf{x}_{inn}) := \left(\frac{\sigma_{11}^2}{X_C} \right)^2 - 1, \tag{41}$$
  3. Matrix Tension:

$$g_4(\mathbf{x}_{inn}) := \frac{(\sigma_{22} + \sigma_{33})^2}{Y_T^2} + \frac{\sigma_{23} - \sigma_{22}\sigma_{33}}{S_{23}^2} + \frac{\sigma_{12}^2 + \sigma_{13}^2}{S_{12}^2} - 1,$$

(42)

4. Matrix Compression:

$$g_5(\mathbf{x}_{inn}) := \left[\left(\frac{Y_C}{2S_{23}} \right)^2 - 1 \right] \left(\frac{\sigma_{22} + \sigma_{33}}{Y_C} \right)$$
$$+ \frac{(\sigma_{22} + \sigma_{33})^2}{4S_{23}^2} + \frac{\sigma_{23}^2 - \sigma_{22}\sigma_{33}}{S_{23}^2} + \frac{\sigma_{12}^2 + \sigma_{13}^2}{S_{12}^2} - 1.$$

(43)

In the above formulæ, σ_{ij} represents the generic component of the stress tensor in the material coordinate system. X and Y represent the material strength along x_1 and x_2 axes, respectively; subscripts T and C stand for tensile and compressive loadings, respectively. S_{ij} denotes the material shear strength in the plane $x_i - x_j$. Of course, if all the above expressions are lower than or equal to zero no failure occurs.

- Delamination onset criterion. The delamination onset is determined by means of the mixed mode quadratic criterion as:

$$g_6(\mathbf{x}_{inn}) := \left(\frac{< \sigma_{33} >}{Z_T} \right)^2 + \left(\frac{\sigma_{23}}{S_{23}} \right)^2 + \left(\frac{\sigma_{13}}{S_{13}} \right)^2 - 1,$$

(44)

where $< \sigma_{33} > := \max(0, \sigma_{33})$ is the transverse normal stress in the material coordinate system (which must be considered if and only if σ_{33} is positive, i.e., when it tends to separate adjacent plies). σ_{13} and σ_{23} are the transverse shear stresses, Z_T is the interlaminar normal strength, while S_{13} and S_{23} are the transverse shear strengths. If the above expression is lower than or equal to zero no delamination occurs.

It is noteworthy that the above failure criteria require the assessment of the 3D stress field within each lamina. This task is achieved through local analysis of the ZOI by means of a layer-wise 1D CUF model, which accurately describes the stress field.

The last set of criteria integrated in the problem formulation of the outer optimisation loop is related to the blending requirement among adjacent panels. Consider two adjacent laminates, denoted by subscripts p and q, the former being thicker than the latter, i.e., $n_p > n_q$. As discussed in [42], in the PPs space, the blending requirement between the generic pair of adjacent laminates p and q can be expressed as:

$$g_{blend-0}^{p,q} := \left[\Delta_{pq}(n\rho_0 c_4) \right]^2 + \left[\Delta_{pq}(n\rho_0 s_4) \right]^2 - (n_p - n_q)^2,$$
$$g_{blend-1}^{p,q} := \left[\Delta_{pq}(n\rho_1 c_2) \right]^2 + \left[\Delta_{pq}(n\rho_1 s_2) \right]^2 - (n_p - n_q)^2.$$

(45)

In Eq. (45), operator $\Delta_{pq}(\cdot)$ is equivalent to $\cdot_p - \cdot_q$, while $c_4 = \cos 4\Phi_1^{A^*}, s_4 = \sin 4\Phi_1^{A^*}, c_2 = \cos 2\Phi_1^{A^*}, s_2 = \sin 2\Phi_1^{A^*}$. Of course, the formulæ in Eq. (45) can be expressed in terms of variables α_0
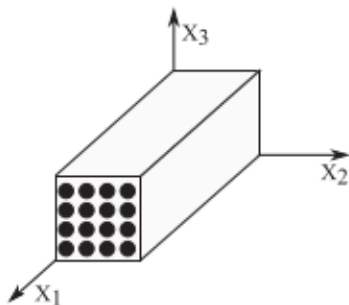

Fig. 6. Local frame orientation for the assessment of first-ply failure and delamination related design requirements.

and α_1 by using the converse relation of Eq. (28). If the above expressions are both lower than or equal to zero, the blending requirement is satisfied.

The least-weight design of the wing-box structure can, now, be formulated as a CNLPP as follows:

$$\min_{\mathbf{x}_{out}} M(\mathbf{x}_{out}),$$

subject to :
$$\begin{cases} [\mathbf{K}_G(\mathbf{x}_{out}) + \lambda(\mathbf{x}_{out})\mathbf{K}_{\sigma G}(\mathbf{x}_{out})]\psi_G(\mathbf{x}_{out}) = \mathbf{0}, \\ \mathbf{K}_G(\mathbf{x}_{out})\mathbf{u}_G(\mathbf{x}_{out}) = \mathbf{f}_G, \\ \mathbf{K}_L(\mathbf{x}_{inn})\mathbf{u}_L(\mathbf{x}_{out}, \mathbf{x}_{inn}) + \bar{\mathbf{K}}_L(\mathbf{x}_{inn})\bar{\mathbf{u}}_L(\mathbf{x}_{out}) = \mathbf{0}, \\ \min_{\mathbf{x}_{inn}} I(f_i(\mathbf{x}_{inn})), \\ g_1(\mathbf{x}_{out}) \leqslant 0, \\ g_j(\mathbf{x}_{inn}) \leqslant 0, \ j = 2, \ldots, 6, \\ g_{blend-i}^{p,q} \leqslant 0, \ i = 0, 1, \ \forall p, q. \end{cases}$$

(46)

It is noteworthy that problem (46) is a non-standard, non-convex CNLPP. The non-convexity is due, on the one hand, to the nature of the constraint functions involved in the problem formulation, and, on the other hand, on the strong coupling between global and local FE models (and, consequently, between the two loops constituting the whole optimisation process). According to the flow-chart illustrated in Fig. 5, one can state that the dependency among the two set of variables of both inner and outer optimisation loops is governed by a sort of strong coupling. On the one hand, the solution of the outer optimisation loop, i.e., $\mathbf{x}_{out}$, depends upon the solution of the SLP (inner optimisation loop), i.e., $\mathbf{x}_{inn}$, through the constraints g_j, $(j = 2, \ldots, 6)$. On the other hand, according to Eq. (31), the solution of the SLP depends upon the value of $\mathbf{x}_{out}$ (recall that the SLP is solved on-the-fly for each individual of the outer optimisation loop).

As stated in Section 4, the ERASMUS code [16] is used to carry out the solution search for both outer and inner optimisation loops. The bounds and the nature of the design variables involved in the outer loop are reported in Table 3, while the design variables of the inner loop have already been discussed in Section 5.3. It is noteworthy that the genotype of the generic individual of the outer optimisation loop is characterised by six chromosomes (one for each panel), each one composed of four genes, where each gene is related to a component of the design variables vector of the outer loop.

As shown in Fig. 5, the GA ERASMUS is coupled, on the one hand, with the ANSYS FE commercial software to calculate the mass, the LFI distribution within the design region and the first buckling factor of the wing-box and, on the other hand, with MUL2@GL code to check the ply-level failure modes of the most critical ZOI. Therefore, for each individual generated by the GA ERASMUS, at each iteration of the outer optimisation loop, three FE analyses are carried out: a static analysis (to assess the LFI distribution) and an eigenvalue buckling analysis on the GFEM of the wing-box structure, and a static analysis on the LFEM of the ZOI to check the first-ply failure and delamination onset. The LFEM requires as input the stacking sequence of the sub-panel, which is not provided by the outer optimisation loop. Accordingly, a further local optimisation (inner loop) is necessary to determine the stack of the ZOI. To this purpose, the SLP of the MS2LOS is solved on-the-fly (for each individual of the outer loop) by means of the ERASMUS algorithm providing, in this way, the optimal stacking sequence in the space of QT solutions. Once the QT SS is obtained, the MUL2@GL code computes the design requirements related to the first-ply failure and to the delamination onset. These software are interfaced by means of a routine programmed in Python language.

Table 3
Bounds on the design variables of the outer optimisation loop.

| Design variable	Type	Lower bound	Upper bound	Discretisation step
α_0	continuous	0.0	1.0	-
α_1	continuous	0.0	1.0	-
n_l	integer	13	30	1
n_g	integer	1	5	1
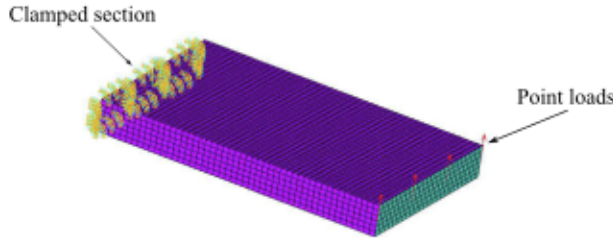
Fig. 7. Mesh and BCs of the GFEM of the wing-box structure.

At each iteration of the outer optimisation loop, the outputs are the value of the objective function and of the constraints functions. ERASMUS elaborates the results provided by the FE analyses to perform the genetic operations. Both inner and outer loops are repeated until the user-defined convergence criteria are satisfied.

Remark 5.1. The SLP of the inner loop is solved on-the-fly only for the ZOI which is located on the most critical panel belonging to the design region. This means that the optimal stacking sequence, which belongs to the class of QT solutions, is calculated on-the-fly only for one laminate of the design region. However, this is not an issue because, at the end of the optimisation process, the stacks of the other panels can be determined through the general strategy presented in [42], which exploits the concept of search propagation direction, on the one hand, to satisfy the blending constraints without introducing simplifying hypotheses on the nature of the stack (e.g., symmetric, balanced, etc.) and, on the other hand, to minimise the discrepancy between the solutions of the FLP and of the SLP.

Remark 5.2. The number of panels composing the design region of the benchmark structure is $n_p = 6$. The number of design variables of the outer optimisation loop is $n_{out} = 4n_p = 24$. The number of design variables of the inner optimisation loop is $n_{inn} = n_g + 1$, thus
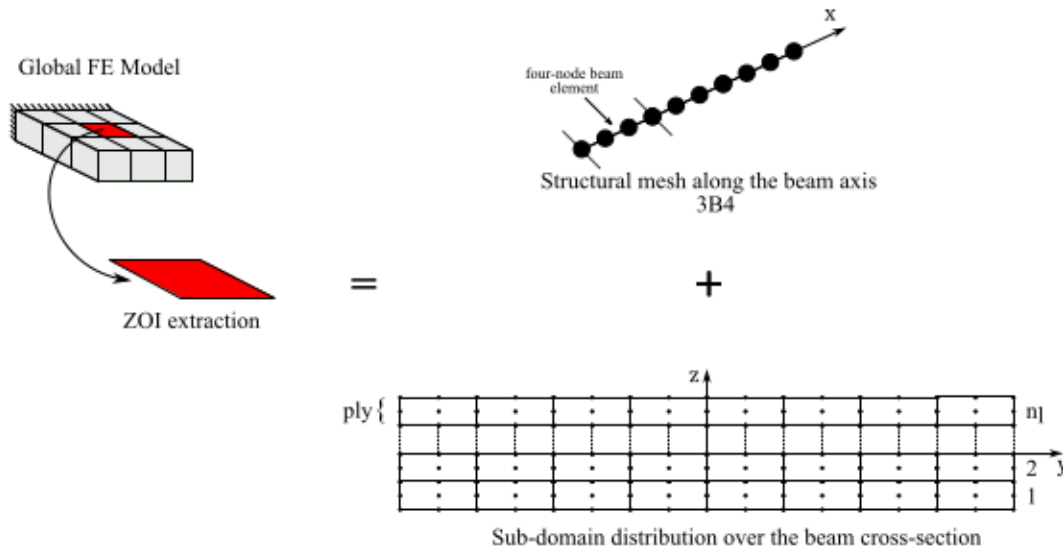
it depends on the current value of the number of saturated groups related to the generic individual of the outer optimisation loop. The overall number of optimisation constraints is $n_{con} = 6 + 2N_{blend}$ where N_{blend} is the number of pairs of adjacent laminates belonging to the design region. For the benchmark structure illustrated in Fig. 4 $N_{blend} = 4$, thus the overall number of optimisation constraints is $n_{con} = 14$.

6. The finite element models

6.1. The global finite element model of the wing-box

Two FE models of the wing-box structure are interfaced with the outer optimisation loop shown in Fig. 5: the GFEM of the whole wing-box and the LFEM of the most critical sub-panel belonging to the design region.

The FE model of the wing-box is automatically generated by means of an ad-hoc ANSYS parametric design language (APDL) script. The geometry and the mesh of the GFEM are opportunely parameterized and depend upon the input variables passed from ERASMUS to the APDL script. The mesh and the BCs of the GFEM are illustrated in Fig. 7. As far as BCs are concerned, $u_j = 0, \theta_j = 0$ ($j = x, y, z$) are set on nodes located at $x = 0$, while four point loads are applied on the nodes located at $x = L$ as discussed in Section 4.

Two analyses are then executed on the GFEM: a static analysis to assess the LFI distribution and an eigenvalue buckling analysis to compute the first buckling factor of the structure. The mesh of the GFEM is composed of four-node ANSYS SHELL181 elements with six degrees of freedom (DOFs) per node (FSDT framework using the implicit definition of the laminate constitutive matrices based on PPs). A mesh convergence analysis, not reported here for the sake of brevity, has been carried out to calibrate the mesh size in order to find a compromise between accuracy and computational costs. As a result of this sensitivity analysis, the element size has been set equal to 80 mm for an overall number of elements $N_{eG} = 4500$.

6.2. Identification of the zone of interest: the laminate-level failure criterion

The identification (and isolation) of the ZOI, which corresponds to one of the sub-panels constituting the design region of the wing-box, as shown in Fig. 4, is done by evaluating the local LFI according

Fig. 8. Layer-wise high-order LFEM.

Table 4
Genetic parameters of the GA ERASMUS for the outer and inner loops.

| | Genetic parameters | |
	Outer loop	Inner loop
N. of populations	1	1
N. of individuals	480	70
N. of generations	500	100
Crossover probability	0.85	0.85
Mutation probability	0.01	0.02
Selection operator	roulette-wheel	tournament selection
Elitism operator	active	active

Table 5
Mass of the reference and the optimised configurations of the wing-box.

	Mass [kg]	Mass reduction %
Reference solution	261	–
Optimised solution, case 1	234.05	10.33
Optimised solution, case 2	243.59	6.67

to the laminate-level failure criterion proposed by Catapano and Montemurro in [3,63] and briefly discussed in Section 2.

Let Ω_{DR} be the set of elements constituting the design region. It is possible to define the maximum LFI as follows:

$$F_{TW,max}^{lam} := \max_{e \in \Omega_{DR}} F_{TW,e}^{lam}, \qquad (47)$$

where $F_{TW,e}^{lam}$ is the LFI of Eq. (15) evaluated at the centroid of each element belonging to Ω_{DR}.

Let e_{max} be the ID of the element having the maximum LFI. Let Ω_{SP_j}, $(j = 1, \ldots, 18)$ be the set of elements constituting the j-th sub-panel of the design region. Of course, $\Omega_{DR} = \bigcup_{j=1,\ldots,18} \Omega_{SP_j}$.

The most critical ZOI corresponds to the j-th sub-panel to which e_{max} belongs. Subsequently, this panel is extracted from the GFEM and meshed by using high-order 1D layer-wise elements as discussed in the following.

6.3. The local finite element model

The LFEM of the most critical ZOI is automatically generated by the Python interface after a post-processing phase of the results of the static analysis conducted on the GFEM. As discussed above, the LFI distribution is used to identify, isolate and extract the most-critical sub-panel of the design region of the wing-box, which constitutes the ZOI to be modelled via high-order theories. Particularly, as illustrated in Fig. 8, the LFEM of the ZOI is composed of three high-order four-node beam elements (B4) belonging to the LE class. The beam cross-section is made of eight L9 sub-domains along the y-axis and one L9 sub-domain per ply along the z axis. BCs of the Dirichlet type are imposed on the LFEM boundary. In particular, the DOFs of the nodes located on the boundary of the most-critical sub-panel are recovered from the results of the static analysis performed on the GFEM and transferred to the LFEM. To correctly ensure the transfer of the BCs from the GFEM to the LFEM

(which are characterised by different meshes and different element types) the DOFs evaluated at the nodes belonging to the skin of the sub-panel of the GFEM are interpolated and transferred to the nodes located on the boundary of the sub-domains of the cross-section of each beam element composing the LFEM (as shown in Fig. 8) according to Eq. (39). Finally, a static analysis is conducted on the LFEM to have an accurate assessment of the local stress field, which is of paramount importance to correctly predict the first-ply failure and the delamination onset according to the criteria of Eqs. (40)–(44). This is the main goal of the LFEM based on high-order beam elements developed in the CUF framework.

7. Numerical results

As stated above, the least-weight design problem of a composite wing-box structure is faced in this study. A modified version of the MS2LOS is employed to solve the problem and the global–local modelling approach based on high-order layer-wise beam theories in the framework of CUF is used to locally verify the failure criteria of the critical ZOI of the wing-box during its optimisation. The aim is to minimise the mass of the structure subject to requirements on different nature, i.e., buckling, strength, delamination, blending, as

(a) Case 1

(b) Case 2

Fig. 9. Mass of the best individual vs. number of generations for the best individual during the optimisation process.
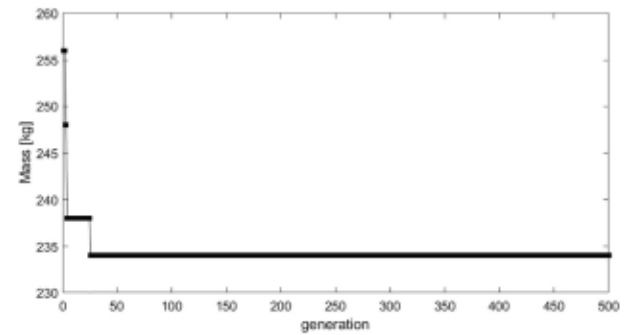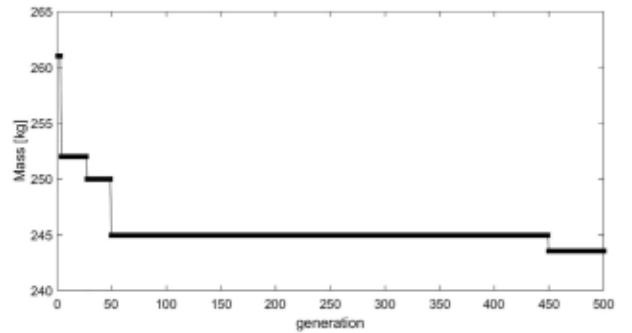
Table 6
Value of the design variables for the best individual of the outer optimisation loop (the dimensionless polar parameters are reported instead of the values of α_0 and α_1).

| | Case 1 | | | | Case 2 | | | |
	ρ_0	ρ_1	n	n_g	ρ_0	ρ_1	n	n_g
Panel 1	0.77	0.91	16	3	0.96	0.06	13	3
Panel 2	0.85	0.58	13	3	0.60	0.15	17	3
Panel 3	0.46	0.08	14	3	0.61	0.26	13	2
Panel 4	0.43	0.14	21	2	0.67	0.29	30	3
Panel 5	0.21	0.32	23	3	0.81	0.31	21	4
Panel 6	−0.67	0.14	16	3	0.00	0.26	15	4

detailed in Eq. (46). Specifically, the CNLPP of Eq. (46) has been solved by considering two different cases: in the first one (referred to as *case 1*) blending constraints are not included in the problem formulation, while in the second one (referred to as *case 2*) they are integrated in the problem formulation.

The genetic parameters tuning the behaviour of the GA ERASMUS utilised to perform the solution search for both outer and inner loops of the optimisation strategy discussed in Section 4.3 are listed in Table 4 for both cases 1 and 2. Regarding the constraint-handling technique used in the outer loop, the ADP method has been considered [79]. For more details on the numerical techniques developed within the new version of ERASMUS and the meaning of the values of the different parameters tuning the algorithm the reader is addressed to [16].
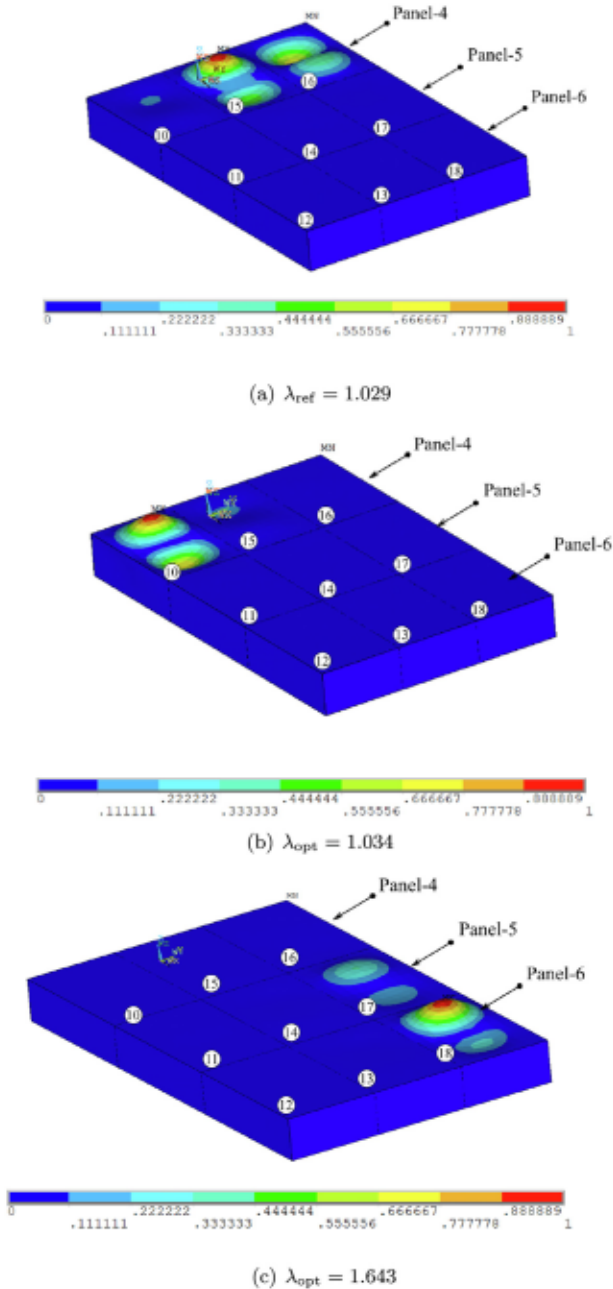
Table 5 lists the mass of the optimised configuration with respect to the reference one for both design cases, whilst Table 6 reports the set of the outer loop design variables for each panel of the wing-box design region for the best individual within the population of the outer loop for cases 1 and 2.

Fig. 9 illustrates the value of the objective function for the best individual (within the population) vs. the number of generations for each design case. One can notice that the convergence towards the optimised configuration of the wing-box is achieved after 25 iterations of the outer loop for case 1 and after 450 for case 2. This is an expected result, which is due to the presence of the blending constraints in the formulation of the CNLPP of Eq. (46). Indeed, the presence of such constraints has an impact on the convergence rate of the algorithm to find a feasible near-optimal solution. Moreover, the integration of the blending requirement among the constraints of the optimisation problem strongly modifies the topology of the feasible region and some near-optimal solutions can be located in small feasible "islands". These solutions can be found only by exploiting the exploration capabilities of the GA through the mutation operator that can produce feasible solutions even at the end of the number of iterations. To this end, when dealing with the blending requirement, the user should strongly increase the maximum number of iterations at the price of higher computational costs.

The mode shape related to the first buckling load, for the reference solution and for the optimised one (for both cases 1 and 2), is shown in Fig. 10, whilst the distribution of the LFI over the elements constituting the design region of the wing-box structure is illustrated in Figs. 11 and 12 for cases 1 and 2, respectively.

From the analysis of these results, it can be immediately inferred that, for both design cases, the most critical zone of the
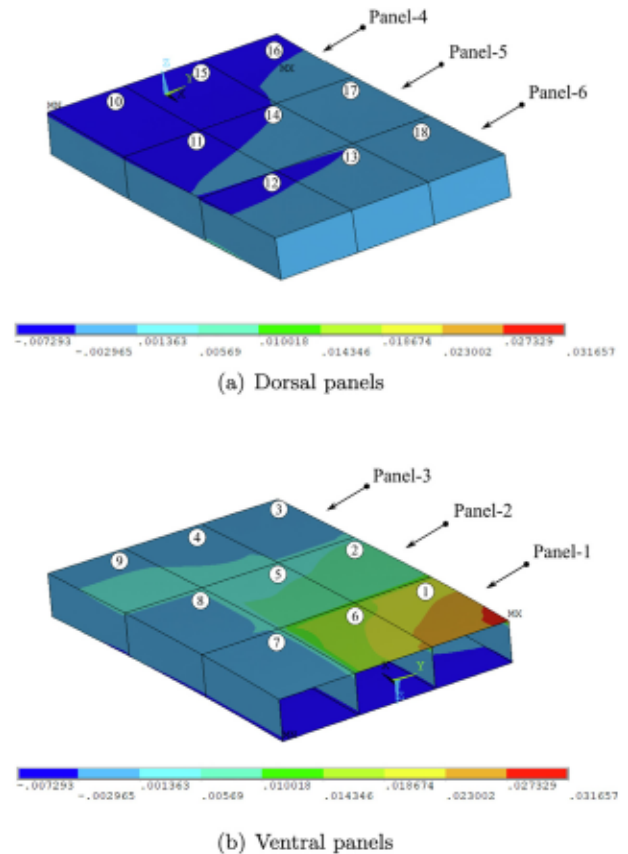

(a) $\lambda_{\text{ref}} = 1.029$

(b) $\lambda_{\text{opt}} = 1.034$

(c) $\lambda_{\text{opt}} = 1.643$

Fig. 10. Mode shape related to the first buckling load for (a) reference solution, (b) optimised solution of case 1 and (c) optimised solution of case 2.

(a) Dorsal panels

(b) Ventral panels

Fig. 11. Distribution of the LFI in the design region of the wing-box structure for the optimised solution of case 1.
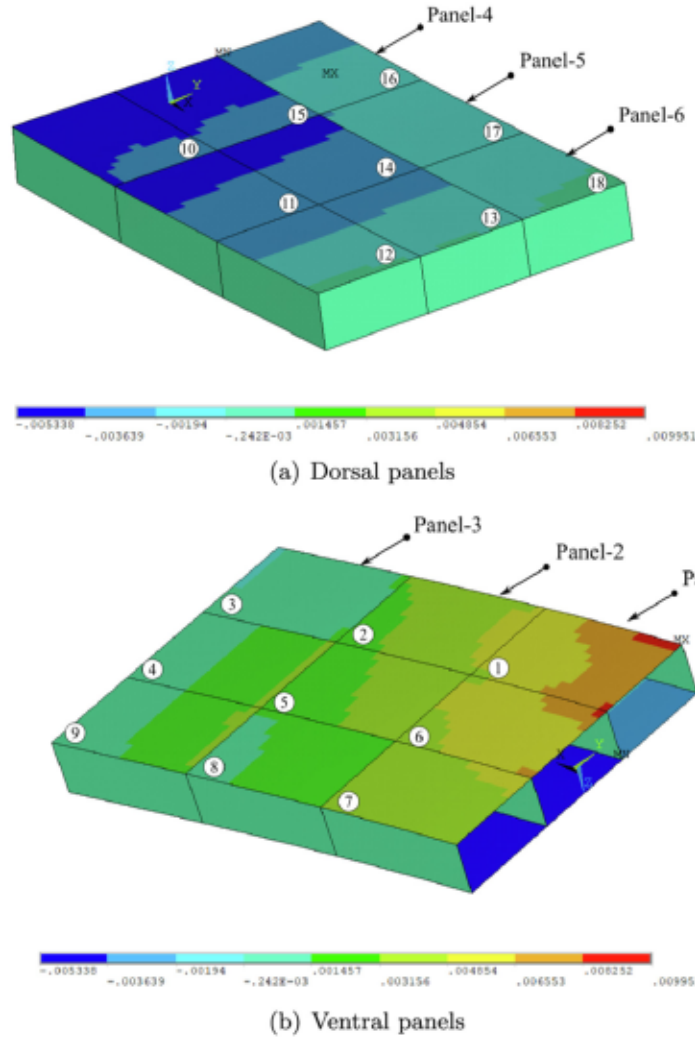
(a) Dorsal panels

(b) Ventral panels

Fig. 12. Distribution of the LFI in the design region of the wing-box structure for the optimised solution of case 2.

Table 7
Optimal value of the design variables of both outer and inner loops of the ZOI (sub-panel 1 in Fig. 4 for both design cases).

Outer loop	Case 1 Inner loop
$\rho_0 = 0.77$	
$\rho_1 = 0.91$	$[2°/-16°/12°/2°/12°/2°/2°/-16°/$
$n = 16$	$-16°/2°/2°/12°/2°/12°/-16°/2°]$
$n_g = 3$	
	Case 2
Outer loop	Inner loop
$\rho_0 = 0.96$	
$\rho_1 = 0.06$	$[87°/7°/-10°/87°/-10°/87°/-10°/$
$n = 13$	$7°/87°/87°/7°/87°/-10°]$
$n_g = 3$	

design region is the sub-panel 1 belonging to panel 1, which is selected as a ZOI (the LFI gets the highest values for some elements belonging to this sub-panel). The values of the design variables of the outer loop at the end of the optimisation process together with the near-optimal stacking sequence found at the end of the inner loop for the ZOI are reported in Table 7 for both design cases, whilst the associated polar diagrams of the homogenised stiffness matrices are depicted in Fig. 13 for case 1 and in Fig. 14 for case 2.

The through-the-thickness variation of the in-plane stress field (σ_{ij}, $i,j = x, y$) evaluated at the centre of the ZOI for the stacks provided in Table 7 is illustrated in Figs. 15 and 16 for cases 1 and 2, respectively. No out-of-plane stresses are represented here because they are negligible whit respect to the in-plane ones.

The following remarks can be drawn from the analysis of these results.

In terms of the first buckling load, the near-optimal solution of case 1 is very close to the reference one and the local buckling occurs in sub-panel 10 of panel 4, whilst in the reference solution the local buckling occurs, essentially, in sub-panels 15 and 16, as illustrated in Fig. 10. Conversely, regarding the near-optimal solution of case 2, the buckling factor is about 60% greater than the one of the reference solution.

As reported in Table 5, the optimised solutions of cases 1 and 2 are 10.33% and 6.67% lighter than the reference one, respectively, which is a quite good achievement and demonstrates the effectiveness of the proposed approach in solving the least-weight design problem for the simplified composite wing-box considered in this study. Of course, the mass of the optimised solution of case 2 is higher than the counterpart of case 1 due to the presence of blending constraints.

(a) First component of homogenised stiffness matrices $\mathbf{A}^*$, $\mathbf{B}^*$ and $\mathbf{D}^*$
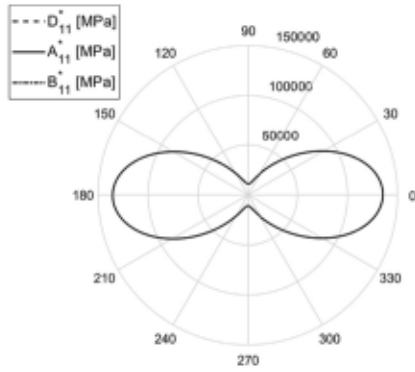
(a) First component of homogenised stiffness matrices $\mathbf{A}^*$, $\mathbf{B}^*$ and $\mathbf{D}^*$

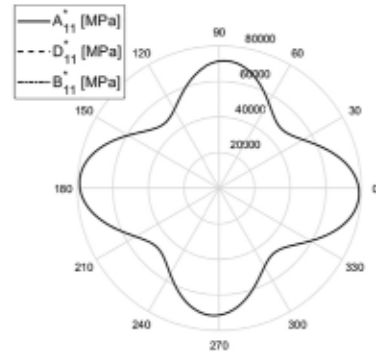(b) Homogenised shear stiffness matrix $\mathbf{H}^*$
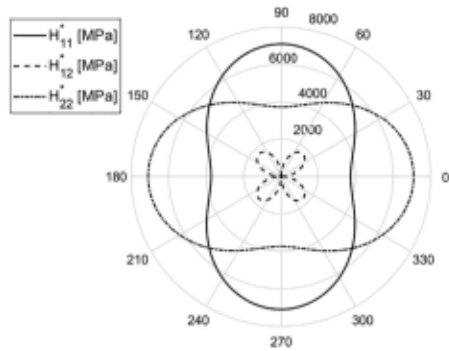
(b) Homogenised shear stiffness matrix $\mathbf{H}^*$

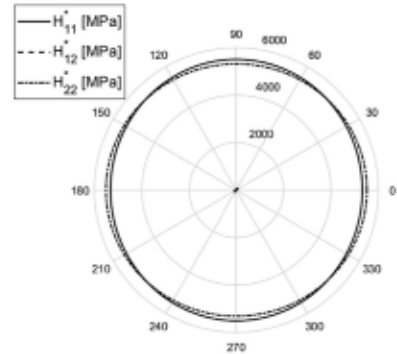**Fig. 13.** Homogenised stiffness matrices of the best individual reported in Table 7, case 1.

Fig. 14. Homogenised stiffness matrices of the best individual reported in Table 7, case 2.

As summarised in Table 6, each panel composing the design region of the solution of case 1 is characterised by a standard orthotropic behaviour (with $K^{\Lambda^*} = 0$ because ρ_0 is positive), except panel 6, which shows the so-called "dog bone" orthotropy (i.e., with $K^{\Lambda^*} = 1$ because ρ_0 is negative). Conversely, regarding the optimised solution of case 2, all panels are characterised by a standard orthotropic behaviour.

Regarding the distribution of the number of layers and of the number of saturated groups (i.e., the number of orientations to be used in defining the QT stacking sequence during the on-the-fly resolution of the SLP in the inner optimisation loop) over the panels constituting the design region, the optimised solutions of cases 1 and 2 reported in Table 6 are quite different and no clear trends can be identified (this is normal when dealing with non-convex multi-modal CNLPPs).

Figs. 13 and 14 highlights two important aspects of the optimal stacking sequence characterising the ZOI for both design cases (listed in Table 7): the solution is perfectly decoupled and homogeneous (thanks to the use of QT solutions), and it is totally orthotropic in membrane and bending (the polar diagram is characterised by two axes of symmetry) with the main axis of orthotropy oriented at $0°$ (a small deviation can be observed for the stacking sequence of the ZOI in design case 2). Particularly, the QT stack found for the ZOI in case 1 is characterised by a standard orthotro-

pic behaviour, whilst the QT solution found for the ZOI in case 2 is characterised by an almost square symmetric behaviour (because the value of ρ_1 is one order of magnitude lower than the value of ρ_0, see Table 6). Accordingly, as discussed in [13], when ρ_1 goes to zero, the transverse shear stiffness matrix exhibits an isotropic behaviour: this is confirmed by the second plot in Fig. 14, where the polar diagram of the components of the transverse shear matrix is almost a circle.

It is noteworthy that these results have been obtained by exploiting the properties of general QT stacks which are neither symmetric nor balanced: this is due to the great potential behind the polar formalism in describing the elastic behaviour of laminates without using symplifying hypotheses on the nature of the stacks.

Finally, although the local analysis of the ZOI through the global–local modelling approach based on high-order layer-wise beam theories allows describing the through-the-thickness variation of the stress field in a way more accurate than commercial FE codes, in the case study considered here, the optimised stack is not characterised by particular issues in terms of first-ply failure and delamination. Particularly, by comparing Figs. 15 and 16, one can notice that in both cases the stresses within the ply are very low and that in case 2 they are almost constant along the through-the-thickness coordinate in each layer (the slope being negligible).

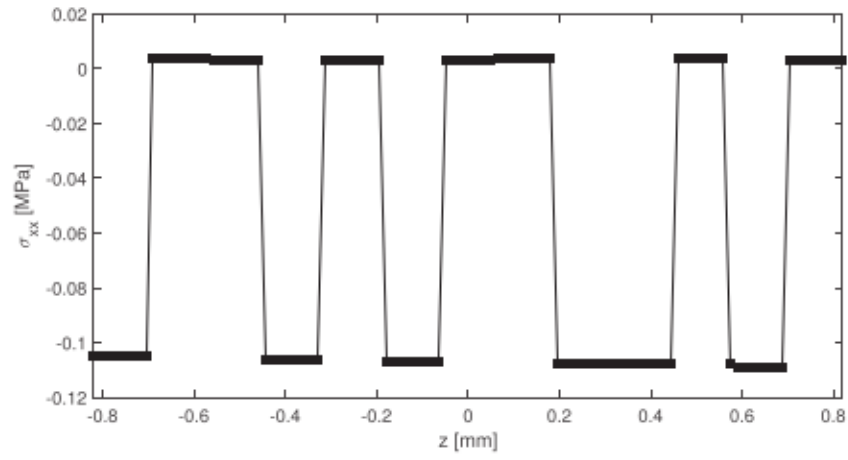(a) σ_{xx} vs. z
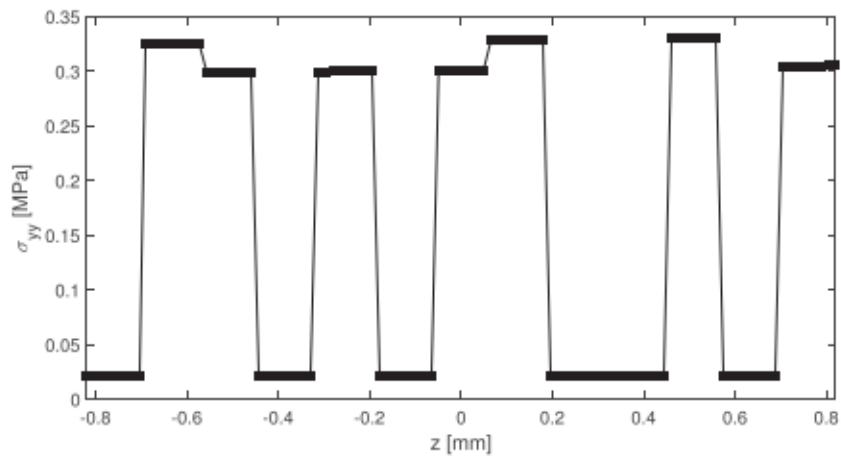

(b) σ_{yy} vs. z
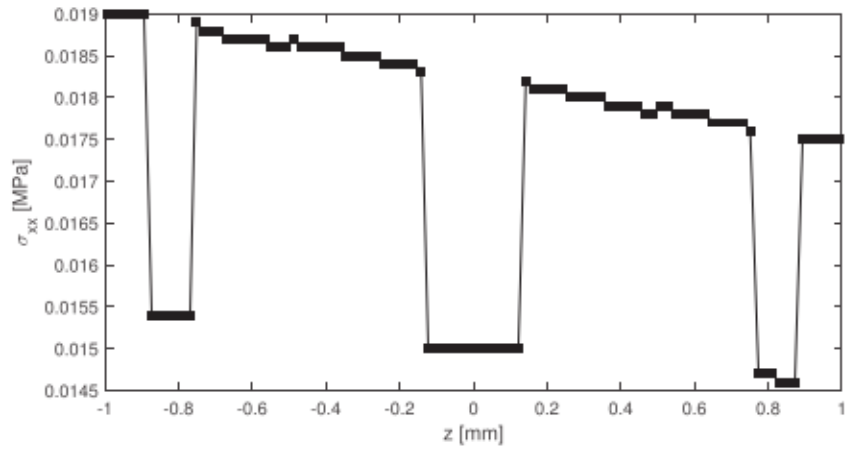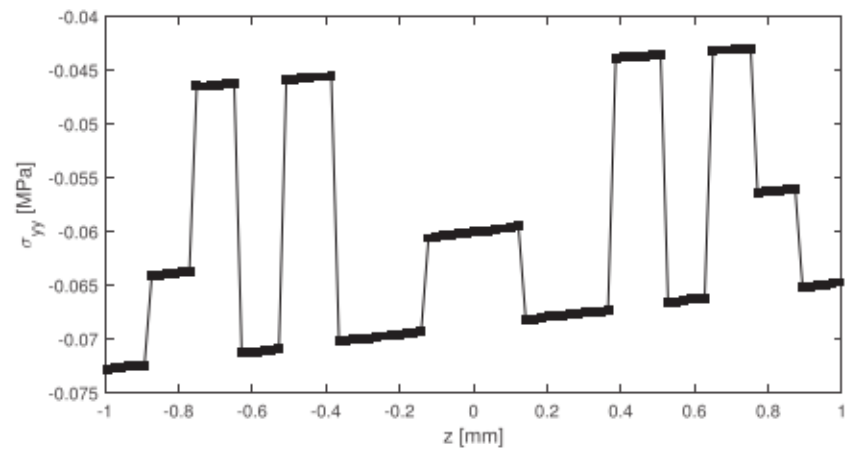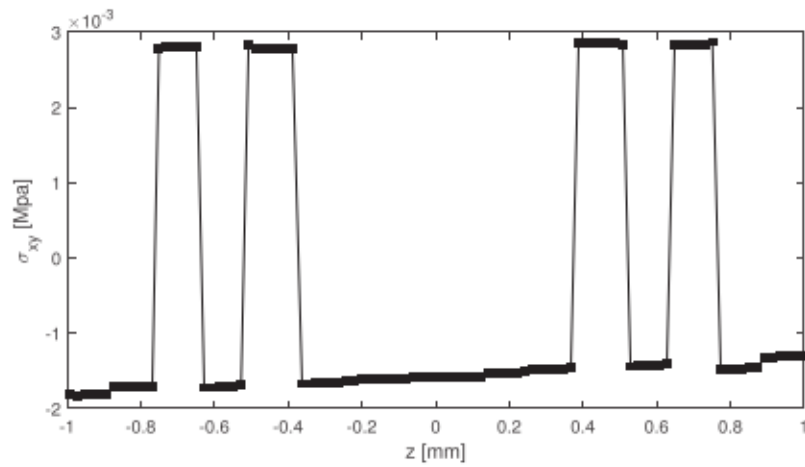
(c) σ_{xy} vs. z

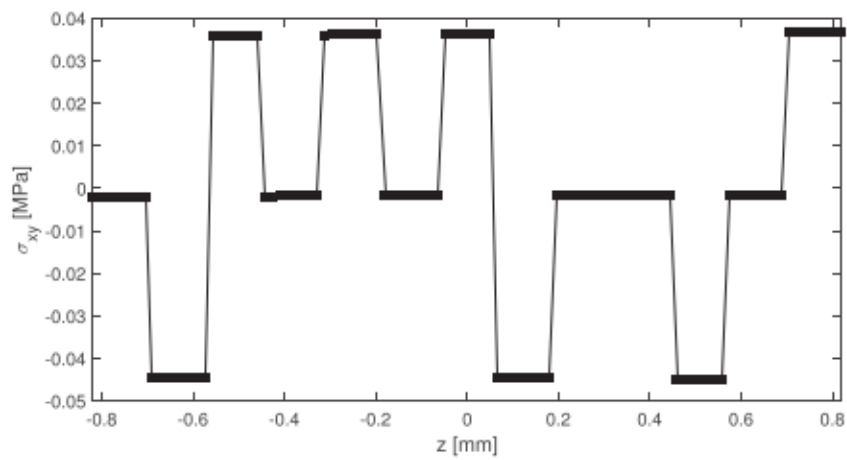**Fig. 15.** Stress field through the thickness at the centre of the ZOI, case 1.

(a) σ_{xx} vs. z

(b) σ_{yy} vs. z

(c) σ_{xy} vs. z

Fig. 16. Stress field through the thickness at the centre of the ZOI, case 2.

8. Conclusions

A modified version of the multi-scale two-level optimisation strategy has been proposed in this work and has been applied to the least-weight design problem of a simplified composite wing-box structure subject to design requirements related to first buckling load, blending constraints, delamination and first-ply failure.

The main contribution of this paper consists in the integration of the global–local modelling approach based on high-order theories within the multi-scale two-level optimisation strategy of composite structures based on polar parameters. This task, which is anything but trivial, implies major modifications on the overall architecture of the optimisation process. Particularly, the first-ply failure and the delamination requirements are checked by using the global–local modelling approach, based on the Carrera's Unified Formulation, through a local layer-wise model whose kinematics relies on high-order beam theories. To this end, the workflow of the optimisation process has been modified to integrate the global–local modelling strategy: this leads to a profound modification of the multi-scale two-level optimisation methodology classically used in the literature because there is no longer a clear distinction between first-level problem (structural optimisation) and second-level problem (lay-up design). Conversely, in the modified version of the multi-scale two-level optimisation strategy, the optimal design of the composite structure is carried out through two nested optimisation loops, referred to as outer and inner loops, which correspond to the first-level and second-level problems, respectively. Moreover, due to the current work-flow there is a sort of strong coupling between the two optimisation loops.

The outer loop deals with the macroscopic scale of the composite structure: at this scale, the behaviour of each laminate constituting the structure is described through the use of polar parameters and geometrical parameters, which constitute the design variables of the outer loop.

The inner loop deals with the mesoscopic scale (i.e., the lamina-level) and focuses on the lay-up design of the most critical region of the composite structure (the so-called zone of interest): the design variables are the layer orientations and the goal is to find a suitable stack matching the current value of the polar parameters and thickness provided by the outer loop. This problem is solved on-the-fly, by considering general stacks belonging to the space of quasi-trivial solutions, without introducing simplifying hypotheses on the nature of the stack, like symmetric stack, balanced stack, etc.

From an optimisation standpoint, there is a strong coupling between the two loops: the solution of the inner loop (the stack of the most critical region) depends on the current values of the design variables of outer loop (i.e., polar parameters and thickness), whilst the solution of the outer loop implicitly depends upon the solution of the inner loop because the requirements on the first-ply failure index and on the delamination are introduced in the problem formulation and checked on the stacking sequence of the zone of interest by means of a global–local modelling strategy based on high-order beam theories.

The optimised solution found for the benchmark structure considered in this study is 10.33% lighter than the reference one, when blending constraints are not integrated in the problem formulation, whilst the weight saving reduces to 6.67% when blending requirement is considered in the problem formulation. In both cases, the optimised solution is characterised by an enhanced buckling strength and meets all the design requirements (in terms of failure criteria and blending constraint), proving, thus, the effectiveness of the proposed approach. Further tests need to be performed to assess the effectiveness of the proposed methodology when dealing with design problems involving complex geometries and multiple loading conditions, by integrating into the problem formulation more complex phenomena like post-buckling behaviour, damage mechanics, etc. The results obtained in this work represent just a first (encouraging) step to develop a general multi-scale optimisation approach to design complex composite structures: research is ongoing in this direction.

9. Data availability

The raw/processed data required to reproduce these findings cannot be shared at this time as the data also forms part of an ongoing study.

Declaration of Competing Interest

The authors declare that they have no known competing financial interests or personal relationships that could have appeared to influence the work reported in this paper.

Acknowledgements

References

[1] Montemurro M, Catapano A. A general b-spline surfaces theoretical framework for optimisation of variable angle-tow laminates. Compos Struct 2019;209:561–78.

[2] Montemurro M, Catapano A. On the effective integration of manufacturability constraints within the multi-scale methodology for designing variable angle-tow laminates. Compos Struct 2017;161:145–59. https://doi.org/10.1016/j.compstruct.2016.11.018.

[3] Catapano A, Montemurro M. Strength optimisation of variable angle-tow composites through a laminate-level failure criterion. J Optim Theory Appl 2020;187:683–706. https://doi.org/10.1007/s10957-020-01750-6.

[4] Izzi MI, Catapano A, Montemurro m. Strength and mass optimisation of variable-stiffness composites in the polar parameters space. Struct Multidiscip Optim 2021;64:2045–73. https://doi.org/10.1007/s00158-021-02963-7.

[5] Fiordilino G, Izzi M, Montemurro M. A general isogeometric polar approach for the optimisation of variable stiffness composites: Application to eigenvalue buckling problems. Mech Mater 2021;153:103574.

[6] Montemurro M, Roiné T, Pailhès J. Multi-scale design of multi-material lattice structures through a CAD-compatible topology optimisation algorithm. Eng Struct 2022;273:115009.

[7] Ghasemi H, Park HS, Rabczuk T. A multi-material level set-based topology optimization of flexoelectric composites. Comput Methods Appl Mech Eng 2018;332:47–62.

[8] Ghiasi H, Pasini D, Lessard L. Optimum stacking sequence design of composite materials part i: Constant stiffness design. Compos Struct 2009;90(1):1–11.

[9] Jones R. Mechanics of composite materials. McGraw-Hill; 1975.

[10] Tsai S, Pagano NJ. Invariant properties of composite materials, Tech. rep., Air force materials lab Wright-Patterson AFB Ohio; 1968.

[11] Tsai S, Hahn T. Introduction to composite materials. Technomic; 1980.

[12] Verchery G. Les Invariants des Tenseurs d'Ordre 4 du Type de l'Élasticité. In: Boehler J-P, editor. Mechanical Behavior of Anisotropic Solids/ Comportment Méchanique des Solides Anisotropes. Netherlands, Dordrecht: Springer; 1982. p. 93–104. https://doi.org/10.1007/978-94-009-6827-1_7.

[13] Montemurro M. An extension of the polar method to the first-order shear deformation theory of laminates. Compos Struct 2015;127:328–39. https://doi.org/10.1016/j.compstruct.2015.03.025.

[14] M. Montemurro, Corrigendum to "an extension of the polar method to the first-order shear deformation theory of laminates" [compos. struct. 127 (2015) 328-339], Composite Structures 131 (2015) 1143–1144. doi:10.1016/j.compstruct.2015.06.002.

[15] Montemurro M. The polar analysis of the third-order shear deformation theory of laminates. Compos Struct 2015;131:775–89. https://doi.org/10.1016/j.compstruct.2015.06.016.

[16] M. Montemurro, A contribution to the development of design strategies for the optimisation of lightweight structures. HDR thesis, Université de Bordeaux,

http://hdl.handle.net/10985/15155, Bordeaux, France, 2018. http://hdl.handle.net/10985/15155.

[17] Irisarri F-X, Lasseigne A, Leroy F-H, Le Riche R. Optimal design of laminated composite structures with ply drops using stacking sequence tables. Compos Struct 2014;107:559–69.

[18] Meddaikar Y, Irisarri F-X, Abdalla M. Laminate optimization of blended composite structures using a modified shepard's method and stacking sequence tables. Struct Multidiscip Optim 2017;55:535–46.

[19] Akbulut M, Sonmez FO. Design optimization of laminated composites using a new variant of simulated annealing. Comput Struct 2011;89(17):1712–24.

[20] Yoo K, Bacarreza O, Aliabadi MF. Multi-fidelity probabilistic optimisation of composite structures under thermomechanical loading using gaussian processes. Comput Struct 2021;257:106655.

[21] Diaconu CG, Sato M, Sekine H. Feasible region in general design space of lamination parameters for laminated composites. AIAA J 2002;40(3):559–65.

[22] Liu B, Haftka R, Trompette P. Maximization of buckling loads of composite panels using flexural lamination parameters. Struct Multidiscip Optim 2004;26(1):28–36.

[23] M. Bloomfield, J. Herencia, P. Weaver, Optimisation of anisotropic composite plates incorporating non-conventional ply orientations, in: 49th AIAA/ASME/ASCE/AHS/ASC Structures, Structural Dynamics, and Materials Conference, 16th AIAA/ASME/AHS Adaptive Structures Conference, 10th AIAA Non-Deterministic Approaches Conference, 9th AIAA Gossamer Spacecraft Forum, 4th AIAA Multidisciplinary Design Optimization Specialists Conference, 2008, p. 1918.

[24] Liu D, Toropov VV. A lamination parameter-based strategy for solving an integer-continuous problem arising in composite optimization. Comput Struct 2013;128:170–4.

[25] Jing Z, Sun Q, Zhang Y, Liang K, Li X. Stacking sequence optimization of doubly-curved laminated composite shallow shells for maximum fundamental frequency by sequential permutation search algorithm. Computers & Structures 2021;252:106560.

[26] H. Ding, B. Xu, Z. Duan, W. Li, X. Huang, A cascadic multilevel optimization framework for the concurrent design of the fiber-reinforced composite structure through the NURBS surface, Engineering with Computers. doi:10.1007/s00366-022-01639-0.

[27] Herencia JE, Weaver PM, Friswell MI. Initial sizing optimisation of anisotropic composite panels with t-shaped stiffeners. Thin-Walled Structures 2008;46(4):399–412.

[28] IJsselmuiden ST, Abdalla MM, Gürdal Z. Implementation of strength-based failure criteria in the lamination parameter design space. AIAA journal 2008;46(7):1826–34.

[29] K.R. Bramsiepe, V. Handojo, Y.M. Meddaikar, M. Schulze, T. Klimmek, Loads and structural optimization process for composite long range transport aircraft configuration, in: 2018 Multidisciplinary Analysis and Optimization Conference, 2018, p. 3572.

[30] Macquart T, Bordogna MT, Lancelot P, De Breuker R. Derivation and application of blending constraints in lamination parameter space for composite optimisation. Compos Struct 2016;135:224–35. https://doi.org/10.1016/j.compstruct.2015.09.016.

[31] Picchi Scardaoni M, Montemurro M. Convex or non-convex? On the nature of the feasible domain of laminates. Eur. J. Mech. A. Solids 2021;85:104112. https://doi.org/10.1016/j.euromechsol.2020.104112.

[32] Albazzan MA, Harik R, Tatting BF, Gürdal Z. Efficient design optimization of nonconventional laminated composites using lamination parameters: A state of the art. Compos Struct 2019;209:362–74.

[33] Montemurro M, Vincenti A, Vannucci P. A two-level procedure for the global optimum design of composite modular structures - Application to the design of an aircraft wing. Part 1: theoretical formulation. J. Optim. Theory Appl. 2012;155(1):1–23.

[34] Montemurro M, Vincenti A, Vannucci P. A two-level procedure for the global optimum design of composite modular structures - Application to the design of an aircraft wing. Part 2: numerical aspects and examples. J. Optim. Theory Appl. 2012;155(1):24–53.

[35] Catapano A, Montemurro M. A multi-scale approach for the optimum design of sandwich plates with honeycomb core. part II: the optimisation strategy. Compos Struct 2014;118:677–90. https://doi.org/10.1016/j.compstruct.2014.07.058.

[36] Catapano A, Montemurro M. A multi-scale approach for the optimum design of sandwich plates with honeycomb core. part i: homogenisation of core properties. Compos Struct 2014;118:664–76. https://doi.org/10.1016/j.compstruct.2014.07.057.

[37] Montemurro M, Pagani A, Fiordilino GA, Pailhès J, Carrera E. A general multi-scale two-level optimisation strategy for designing composite stiffened panels. Compos Struct 2018;201:968–79.

[38] Montemurro M, Izzi M, El-Yagoubi J, Fanteria D. Least-weight composite plates with unconventional stacking sequences: Design, analysis and experiments. J. Compos. Mater. 2019;53(16):2209–27. https://doi.org/10.1177/0021998318824783.

[39] Panettieri E, Montemurro M, Catapano A. Blending constraints for composite laminates in polar parameters space. Composites Part B: Engineering 2019;168:448–57.

[40] Izzi M, Montemurro M, Catapano A, Pailhès J. A multi-scale two-level optimisation strategy integrating a global/local modelling approach for composite structures. Compos Struct 2020;237:111908. https://doi.org/10.1016/j.compstruct.2020.111908.

[41] Picchi Scardaoni M, Montemurro M. A general global-local modelling framework for the deterministic optimisation of composite structures. Struct Multidiscip Optim 2020;62:1927–49.

[42] Picchi Scardaoni M, Montemurro M, Panettieri E, Catapano A. New blending constraints and a stack-recovery strategy for the multi-scale design of composite laminates. Struct Multidiscip Optim 2021;63(2):741–66.

[43] Bathe K-J. Finite element procedures. Klaus-Jurgen Bathe; 2006.

[44] Fish J, Pan L, Belsky V, Gomaa S. Unstructured multigrid method for shells. Int. J. Numer. Meth. Eng. 1996;39(7):1181–97.

[45] Moës N, Dolbow J, Belytschko T. A finite element method for crack growth without remeshing. Int. J. Numer. Meth. Eng. 1999;46(1):131–50.

[46] Fish J. The s-version of the finite element method. Computers & Structures 1992;43(3):539–47.

[47] Fish J, Markolefas S. Adaptive s-method for linear elastostatics. Comput. Methods Appl. Mech. Eng. 1993;104(3):363–96.

[48] Shim KW, Monaghan DJ, Armstrong CG. Mixed dimensional coupling in finite element stress analysis. Engineering with Computers 2002;18(3):241–52.

[49] Blanco P, Feijóo R, Urquiza S. A variational approach for coupling kinematically incompatible structural models. Int. J. Numer. Meth. Eng. 2008;197(17–18):1577–602.

[50] Mao K, Sun C. A refined global-local finite element analysis method. Int. J. Numer. Meth. Eng. 1991;32(1):29–43.

[51] Dhia HB. Multiscale mechanical problems: the Arlequin method, Comptes Rendus de l'Academie des Sciences Series IIB Mechanics Physics. Astron. 1998;12(326):899–904.

[52] Hu H, Belouettar S, Potier-Ferry M, et al. Multi-scale modelling of sandwich structures using the Arlequin method part i: Linear modelling. Finite Elem. Anal. Des. 2008;45(1):37–51.

[53] Guyan RJ. Reduction of stiffness and mass matrices. AIAA Journal 1965;3(2):380.

[54] A. Arrieta, A.G. Stritz, Optimal design of aircraft structures with damage tolerance requirements, Struct Multidisc Optim. 30. doi:10.1007/s00158-004-0510-0.

[55] Ciampa PD, Nagel B, Tooren M. Global local structural optimization of transportation aircraft wings. In: in: 51st AIAA/ASME/ASCE/AHS/ASC Structures, Structural Dynamics, and Materials Conference. American Institute of Aeronautics and Astronautics; 2010. https://doi.org/10.2514/6.2010-3098.

[56] V. Chedrik, Two-level design optimization of aircraft structures under stress, buckling and aeroelasticity constraints, in: 10th World Congress on Structural and Multidisciplinary Optimisation, 2013.

[57] Liu Q, Jrad M, Mulani SB, Kapania RK. Integrated global wing and local panel optimization of aircraft wing. In: in: 56th AIAA/ASCE/AHS/ASC Structures, Structural Dynamics, and Materials Conference. American Institute of Aeronautics and Astronautics; 2015. https://doi.org/10.2514/6.2015-0137.

[58] Panettieri E, Montemurro M, Fanteria D, Coccia F. Multi-scale least-weight design of a wing-box through a global/local modelling approach. J. Optim. Theory Appl. 2020:1–24.

[59] Izzi MI, Montemurro M, Catapano A, Fanteria D, Pailhes J. Multi-scale optimisation of thin-walled structures by considering a global/local modelling approach. Proceedings of the Institution of Mechanical Engineers, Part G: Journal of Aerospace Engineering 2020;235(2):171–88.

[60] Picchi Scardaoni M, Montemurro M, Panettieri E. Prandtlplane wing-box least-weight design: a multi-scale optimisation approach. Aerosp. Sci. Technol. 2020;106:106156.

[61] Picchi Scardaoni M, Izzi MI, Montemurro M, Panettieri E, Cipolla V, Binante V. Multiscale Deterministic Optimisation of Blended Composite Structures: Case Study of a Box-Wing. Thin-Walled Structures 2022;170:108521.

[62] Carrera E, Fiordilino G, Nagaraj M, Pagani A, Montemurro M. A global/local approach based on cuf for the accurate and efficient analysis of metallic and composite structures. Eng. Struct. 2019;188:188–201.

[63] Catapano A, Montemurro M. On the correlation between stiffness and strength properties of anisotropic laminates. Mech. Adv. Mater. Struct. 2019;26(8):651–60. https://doi.org/10.1080/15376494.2017.1410906.

[64] Garulli T, Catapano A, Montemurro M, Jumel J, Fanteria D. Quasi-trivial stacking sequences for the design of thick laminates. Compos Struct 2018;200:614–23. https://doi.org/10.1016/j.compstruct.2018.05.120.

[65] Vannucci P, Verchery G. A special class of uncoupled and quasi-homogeneous laminates. Compos. Sci. Technol. 2001;61(10):1465–73. https://doi.org/10.1016/S0266-3538(01)00039-2.

[66] Vannucci P. Plane Anisotropy by the Polar Method. Meccanica 2005;40(4–6):437–54. https://doi.org/10.1007/s11012-005-2132-z.

[67] Reddy JN. Mechanics of composite laminated plates and shells: theory and analysis, Boca Raton. FL: CRC Press; 2003.

[68] Tsai S, Wu E. A General Theory of Strength for Anisotropic Materials. J. Compos. Mater. 1971;5(1):58–80. https://doi.org/10.1177/002199837100500106.

[69] Khani A, IJsselmuiden S, Abdalla M, Gürdal Z. Design of variable stiffness panels for maximum strength using lamination parameters. Composites Part B: Engineering 2011;42(3):546–52. https://doi.org/10.1016/j.compositesb.2010.11.005.

[70] Carrera E, Giunta G, Petrolo M. Beam structures: classical and advanced theories. John Wiley & Sons; 2011.

[71] Carrera E, Cinefra M, Petrolo M, Zappino E. Finite element analysis of structures through unified formulation. John Wiley & Sons; 2014.

[72] Carrera E, Fiordilino G, Nagaraj M, Pagani A, Montemurro M. A global/local approach based on cuf for the accurate and efficient analysis of metallic and composite structures. Eng. Struct. 2019;188:188–201.

[73] Catapano A, Montemurro M, Balcou J-A, Panettieri E. Rapid Prototyping of Variable Angle-Tow Composites. Aerotecnica Missili & Spazio 2019;98 (4):257–71. https://doi.org/10.1007/s42496-019-00019-0.

[74] Vannucci P. A Note on the Elastic and Geometric Bounds for Composite Laminates. J. Elast. 2013;112(2):199–215. https://doi.org/10.1007/s10659-012-9406-1.

[75] Montemurro M, Catapano A, Doroszewski D. A multi-scale approach for the simultaneous shape and material optimisation of sandwich panels with cellular core. Composites Part B: Engineering 2016;91:458–72. https://doi.org/10.1016/j.compositesb.2016.01.030.

[76] Audoux Y, Montemurro M, Pailhès J. A Metamodel Based on Non-Uniform Rational Basis Spline Hyper-Surfaces for Optimisation of Composite Structures. Compos Struct 2020;247:112439. https://doi.org/10.1016/j.compstruct.2020.112439.

[77] Z. Hashin, Failure criteria for unidirectional fiber composites.

[78] Brewer JC, Lagace PA. Quadratic stress criterion for initiation of delamination. J Compos Mater 1988;22(12):1141–55.

[79] Montemurro M, Vincenti A, Vannucci P. The automatic dynamic penalisation method (ADP) for handling constraints with genetic algorithms. Comput Methods Appl Mech Eng 2013;256:70–87.